 doi:10.20944/preprints201701.0086.v3

The Spermine Phosphate-Bound Cyclooctaoxygen Sodium Epigenetic Shell of Euchromatin DNA Is Destroyed by the Epigenetic Poison Glyphosate

Andreas J. Kesel [1,*]

[1]*Chammünsterstr. 47, München 81827, Germany*

***Corresponding author:** Andreas Johannes Kesel, Chammünsterstr. 47, D-81827 München, Germany, Tel: +49 (0)89-453 64 500; E-mail: andreas.kesel@gmx.de

Preprints (www.preprints.org) | NOT PEER-REVIEWED | Posted: 4 December 2017 doi:10.20944/preprints201701.0086.v3

Abstract

Oxygen exists in two gaseous and six solid allotropic modifications. An additional allotropic modification of oxygen, the cyclooctaoxygen, was predicted to exist in 1990. The first synthesis and characterization of cyclooctaoxygen as its sodium crown complex, isolated in the form of three cytosine nucleoside hydrochloride complexes, was reported in 2016. Cyclooctaoxygen sodium was synthesized from atmospheric oxygen, or catalase effect-generated oxygen, under catalysis of cytosine nucleosides and either ninhydrin or eukaryotic low-molecular weight RNA. The cationic cyclooctaoxygen sodium complex was shown to bind RNA and DNA, to associate with single-stranded DNA and spermine phosphate, and to be essentially non-toxic to cultured mammalian cells at 0.1–1.0 mM concentration. We postulated that cyclooctaoxygen is formed in most eukaryotic cells from dihydrogen peroxide in a catalase reaction catalysed by cytidine and RNA. A molecular biological model was deduced for a first epigenetic shell of eukaryotic euchromatin. This model incorporates an epigenetic explanation for the interactions of the essential micronutrient selenium (as selenite) with eukaryotic euchromatin. The sperminium phosphate/cyclooctaoxygen sodium complex is calculated to cover the actively transcribed regions (2.6%) of bovine lymphocyte interphase genome. Cyclooctaoxygen seems to be naturally absent in hypoxia-induced highly condensed chromatin, taken as a model for eukaryotic metaphase/anaphase/early telophase mitotic chromatin. We hence propose that the cyclooctaoxygen sodium-bridged spermine phosphate and selenite coverage serves as an epigenetic shell of actively transcribed gene regions in eukaryotic ‘open’ euchromatin DNA. The total herbicide glyphosate (ROUNDUP) and its metabolite

Preprints (www.preprints.org) | NOT PEER-REVIEWED | Posted: 4 December 2017 doi:10.20944/preprints201701.0086.v3

(aminomethyl)phosphonic acid (AMPA) are proved to represent 'epigenetic poisons', since they both selectively destroy the cyclooctaoxygen sodium complex. This definition is of reason, since the destruction of cyclooctaoxygen is sufficient to bring the protection shield of human euchromatin into collateral epigenetic collapse.

Keywords: spermine; cyclooctaoxygen; DNA; selenium; glyphosate; AMPA

Introduction

In 1677 *Antoni van Leeuwenhoek* discovered [1] the characteristic crystals of spermine phosphate (spermine × 2 H_3PO_4 × 6 H_2O) [2] in matured native human semen (Figure 1). Since then, there was collected conclusive evidence that human chromosomal DNA is closely associated with spermine phosphate [2]. The interaction of oxygen species with DNA has until recently only being focused on oxidative DNA damage and its pathophysiological consequences [3]. In 2015 *Kirmes et al.* reported an unprecedented interaction of eukaryotic chromatin DNA structure with atmospheric oxygen partial pressure [4]. Under switching to hypoxic conditions (1% O_2, 5% CO_2, 94% N_2) the murine cardiomyocyte HL-1 cell chromatin rendered itself highly condensed, accompanied by redistribution of the polyamine pool (mainly spermine and spermidine) to the nucleus [4]. In 2016 *Kesel et al.* showed [5] that eukaryotic single-stranded DNA (ssDNA) binds a new allotropic form of oxygen, the cyclooctaoxygen (cyclo-O_8), in form of its sodium (Na^+) complex (cyclo-O_8-Na^+), especially when in coordination to spermine phosphate (sperminium phosphate) [5]. A model for a logically

Preprints (www.preprints.org) | NOT PEER-REVIEWED | Posted: 4 December 2017 doi:10.20944/preprints201701.0086.v3

resulting first epigenetic shell of eukaryotic DNA *in vivo* was proposed [5]. Also a partial substitution of the sperminium ($C_{10}H_{30}N_4^{4+}$)-bound monohydrogen phosphate (HPO_4^{2-}) anions by hydrogen selenite ($HSeO_3^-$) anions was postulated during these investigations [5], thereby providing an explanation for the well-known, but 'mysterious' [6], augmenting effects of the essential micronutrient selenium on eukaryotic genome integrity and chromosomal DNA stability [6,7].

Materials and Methods

Materials

The following materials were utilized: **NC** ($C_9H_{14}ClN_3O_5 \times 2\ ClNaO_8 \times 2\ H_2O \times ½\ C_3H_6O$) = [tetrakis(*β*-D-cytidin-N^3-ium)(octoxocane-κ^4O^1,O^3,O^5,O^7)]sodium(5+) pentachloride dihydrate hemiacetonate (*M* = 1370.22 g/mol) [5]; **RC** ($C_9H_{14}ClN_3O_5 \times 2\ HClNa_2O_{17} \times ¼\ C_3H_6O$) = *β*-D-cytidine hydrochloride – *μ*-chloro(*μ*-hydroxy)bis(octoxocane-κ^4O^1,O^3,O^5,O^7)disodium (1:2) × 0.25 acetone (*M* = 1003.06 g/mol) [5]; potassium iodide (KI) *puriss. p.a.*, reag. ISO, reag. Ph.Eur., *w* (*m*/*m*) ≥ 99.5% (*M* = 166.00 g/mol) [Sigma-Aldrich Corp., St. Louis, MO, USA; pH 6.0–9.0 [20 °C, 5% (*m*/*m*) in H_2O], loss on drying ≤ 0.2% (105 °C), total nitrogen (N) ≤ 0.001%, heavy metals (as Pb) ≤ 0.0005%, iodate (IO_3^-) ≤ 2 mg/kg]; starch *puriss. p.a.*, from potato, reag. ISO, reag. Ph.Eur., soluble [Sigma-Aldrich Corp., St. Louis, MO, USA; pH 6.0–7.5, loss on drying ≤ 13% (105 °C), sulfated ash ≤ 0.5%, substances reducing *Fehling* solution (as maltose) ≤ 0.7 %]; (aminomethyl)phosphonic acid (AMPA) (CH_6NO_3P, *M* = 111.04 g/mol) [Sigma-Aldrich Corp., St. Louis, MO, USA, Lot: MKBX8824V; *w* (*m*/*m*) = 98.5% (titration), carbon (C) 10.9%, nitrogen (N) 12.6%]; *N*-(phosphonomethyl)glycine

Preprints (www.preprints.org) | NOT PEER-REVIEWED | Posted: 4 December 2017 doi:10.20944/preprints201701.0086.v3

(glyphosate) ($C_3H_8NO_5P$, M = 169.07 g/mol) [Sigma-Aldrich Corp., St. Louis, MO, USA, Lot: MKBX1937V; w (n/n) > 99% (TLC), carbon (C) 21.3%, nitrogen (N) 8.2%, mp 230 °C (dec.)]; deuterated chloroform ($CDCl_3$) [euriso-top®, Saint Aubin cedex, France, Lot: D007H, W2631; 99.80% D, H_2O < 0.01%, stored over molecular sieve 3Å]; molecular sieve 3Å (0.3 nm, zeolithe, metal-aluminosilicate) [AppliChem GmbH, Darmstadt, Germany; Lot: 5H002478; water absorbency ≥ 20% (24 h, 80% humidity)]; elemental iodine I_2 (M = 253.81 g/mol) (iodum resublimatum Ph.Eur. 7.0) [Caesar & Loretz (Caelo) GmbH, Hilden, Germany, Lot: 122890; w (m/m) = 99.9% (titration), non-volatile matter ≤ 0.1%, Br^- and Cl^- ≤ 250 ppm]. L-Ascorbic acid (vitamin C) Ph.Eur. 7.0 (M = 176.12 g/mol) was purchased from a local pharmacy store (Friedens-Apotheke, München-Trudering, Germany). Glyphosate monosodium salt ($C_3H_7NNaO_5P$, M = 191.05 g/mol) was purchased in form of ROUNDUP® GRAN 15,5 g granules [Monsanto Europe S.A., Antwerp, Belgium, Lot: T346 (prod. date 12/12/2011); contains 475 g/kg glyphosate-Na, $w_{glyphosate\text{-}Na}$ (m/m) = 47.5%, inert carrier material 33.5%, water and excipients 19%].

Calculation of the genomic coverage by the cyclooctaoxygen sodium-bridged spermine phosphate epigenetic shell of interphase DNA in bovine lymphocytes

The average volume of human lymphocytes was taken as 206 fl (femtoliter) [8]. The average volume of bovine lymphocytes was taken as 214 fl (femtoliter) after introducing a technical correction factor of f = 0.834 [9]. The reference genome size of *Bos taurus* (Hereford breed) was taken as 2,670,139,648 bp (RefSeq assembly accession number GCF_000003055.6) [10]. This genome showed 41.89% GC content

[10]. The theoretical intracellular concentration of the sperminium phosphate/cyclo-O_8-Na^+ complex required to cover all triplets of the dsDNA genome in a blood lymphocyte of *B. taurus* was calculated: [214 fl × 6.022140857 × 10^{23} mol^{-1}]$^{-1}$ × 2,670,139,648 × 2 × 3^{-1} = 7.7597 pM × 1,780,093,099 = 13.8127 mM. The coverage of *B. taurus* genome by the sperminium phosphate/cyclo-O_8-Na^+ complex was calculated (mean ± s.d.: 2.6208 ± 0.4953%) from the published [11] fractions of spermine bound to dsDNA: 421 μM × [13.8127 mM]$^{-1}$ = 3.0479% (in presence of 2 mM Mg^{2+} and 100 mM K^+), 287 μM × [13.8127 mM]$^{-1}$ = 2.0778% (2 mM Mg^{2+}, 150 mM K^+), and 378 μM × [13.8127 mM]$^{-1}$ = 2.7366% (10 mM Mg^{2+}, 100 mM K^+). The number of base pairs for the number of protein-coding exons in *B. taurus* genome (49,107) [10] was calculated with the median of amino acid residues/gene (468) [10]: 49,107 × 3 bp × 468 = 68,946,228 bp (2.5821% of *B. taurus* genome). The GC content of *E. coli*-derived pBR322 plasmid covalently closed circular dsDNA (GenBank accession number J01749.1) was calculated from its sequence as 53.75%.

Calculation of the spermine coverage of highly condensed mitotic metaphase DNA in HeLa S3 cells

The average effective molecular mass of dGp/dCp was calculated as *M* = 309.19 g/mol, of dAp/dTp as *M* = 308.70 g/mol. The reference *Homo sapiens* genome size was taken as 3,238,442,024 bp (RefSeq assembly accession number GCF_000001405.35) [12]. This genome showed 41.46% GC content [12]. The molecular mass of this human genome dsDNA was calculated: (0.4146 × 309.19 g/mol) + (0.5854 × 308.70 g/mol) × (3,238,442,024 bp × 2) = 2.000730 × 10^{12} g/mol. The HeLa cell genome [13] was

Preprints (www.preprints.org) | NOT PEER-REVIEWED | Posted: 4 December 2017 doi:10.20944/preprints201701.0086.v3

anticipated as 76 chromosomes (hypertriploid) + 22 abnormal chromosomes [13,14]. The chromosomal DNA size of HeLa metaphase chromatin dsDNA was calculated as 19,539,129,390 bp with M = 1.207127414 × 10^{13} g/mol from published karyotyping [14]. The content of spermine in HeLa S3 cell metaphase chromatin was taken as 135.9 ± 16.1 pmol/µg DNA [15]. This was transformed into 135.9 ± 16.1 p(ico)mol spermine/82.84129651 z(epto)mol dsDNA = 1,640,486,155 (molecules spermine/dsDNA). Since one spermine molecule is assumed to cover six bp (in the pure spermine form of A-DNA duplex [16] and Z-DNA duplex [17]), this corresponds to a coverage of 1,640,486,155 × 6 × $[19,539,129,390]^{-1}$ = 50.3754% of HeLa S3 cell metaphase chromatin dsDNA genome by spermine. The content of spermidine in HeLa S3 cell metaphase chromatin was taken as 116.1 ± 11.8 pmol/µg DNA [15]. This was transformed into 116.1 ± 11.8 p(ico)mol spermidine/82.84129651 z(epto)mol dsDNA = 1,401,474,927 (molecules spermidine/dsDNA). Since one spermidine molecule is assumed to cover six bp (in the pure spermidine form of Z-DNA duplex [18,19]), this corresponds to a coverage of 1,401,474,927 × 6 × $[19,539,129,390]^{-1}$ = 43.0359% of HeLa S3 cell metaphase chromatin dsDNA genome by spermidine. Taken together, the polyamine (spermine/spermidine ratio 1.17) coverage of HeLa S3 cell metaphase chromatin dsDNA is 50.3754% + 43.0359% = 93.4113%.

Calculation of the polyamine coverage of maximally condensed mitotic late anaphase/early telophase DNA in murine cryptal enterocytes

Preprints (www.preprints.org) | NOT PEER-REVIEWED | Posted: 4 December 2017 doi:10.20944/preprints201701.0086.v3

The phosphorus (P) content of female *Mus musculus* strain C3H/HeJ cryptal enterocytic mitotic (late anaphase/early telophase) chromatin was taken as 298.5 ± 17.3 mmol (P)/kg [20]. The average effective molecular mass of one nucleotide unit (dGp/dCp and dAp/dTp) in *M. musculus* C3H/HeJ genome (2,701,131,316 bp) [21] was calculated with the GC content of 42.82% [21]: M = 308.91 g/mol. With the formula w (P) = (n_P) × M^{-1} (n_P, number of P atoms *pro* formula unit; M, molecular weight of formula unit) the phosphorus content w (P) of murine mitotic chromatin was calculated: 3,237.19 mmol (P)/kg (free dsDNA). The value for complete complexation with one spermine tetracation/six nucleotides is 2,912.86 mmol (P)/kg (spermine tetracation-complexed ssDNA), and for complete complexation with one spermidine trication/six nucleotides is 2,997.41 mmol (P)/kg (spermidine trication-complexed ssDNA). Taking the arithmetic mean of the published [11,22] spermine/spermidine ratio 0.85, bound to rat liver DNA and RNA (2 mM Mg^{2+}, 150 mM K^{+}) [11], or in *Sprague–Dawley* rat liver nuclei [22], the theoretical value for complete complexation is {(2,912.86 × 0.85) + [(2,997.41 × (2 – 0.85)]} × 2^{-1} = 2,961.48 (P)/kg (spermine tetracation/spermidine trication-complexed ssDNA). Phosphatidylcholine in its dipalmitoyl ($C_{16:0}$) lipid composition (M = 734.04 g/mol) is the main constituent (60.8 ± 1.3%) of the phospholipid fraction in rat liver chromatin [23]. This molecular weight was corrected to an average effective molecular mass M = 765.03 g/mol, based on the fractions [23] and lipid compositions [23] of phospholipids (phosphatidylcholine, phosphatidylethanolamine, phosphatidylserine, phosphatidylinositol, sphingomyelin) in *Sprague–Dawley* rat liver chromatin, to yield the reference value for the (P) content of phospholipid 1,307.13 mmol (P)/kg. The fractions of DNA (32.0 ± 4.1%), RNA (5.1 ± 1.6%), protein (62.6 ± 3.8%), and phospholipid (0.2 ±

Preprints (www.preprints.org) | NOT PEER-REVIEWED | Posted: 4 December 2017 doi:10.20944/preprints201701.0086.v3

0.1%) in *Sprague–Dawley* rat liver chromatin were taken as published [23], and applied on the murine mitotic chromatin nucleic acids (DNA + RNA). The published [20] value was corrected for the chromatin-bound cation (Na^+, K^+, Mg^{2+}, Ca^{2+}) [20], protein and phospholipid [23] content: {[841.0 mmol (Na^+, K^+, Mg^{2+}, Ca^{2+})/kg + 298.5 mmol (P)/kg] × 100 × 37.1^{-1}} + [0.2 × 100^{-1} × 1,307.13 mmol (P)/kg] = 3,074.04 mmol (P)/kg (ssDNA + ssRNA) in mitotic late anaphase/early telophase chromatin. The six nucleotide coverage (ssDNA + ssRNA) by the polyammonium cations was calculated: (3,237.19 – 3,074.04) × $(3,237.19 – 2,961.48)^{-1}$ × 100% = 59.1745%. The genomic dsDNA six bp coverage by the polyammonium cations, corrected for the nuclear RNA content, was calculated: 59.1745% × (32.0 × 37.1^{-1}) × 2 = 102.0800%. This corresponds to a coverage of 5.8777 bp murine cryptal enterocytic mitotic (late anaphase/early telophase) chromatin dsDNA by one polyammonium cation (spermine/spermidine ratio 0.85). The six nucleotide coverage of nuclear RNA by the polyammonium cations was calculated: 59.1745% – (102.0800% × 2^{-1}) = 8.1345%, corresponding to a relative six nucleotide coverage of nuclear RNA: 8.1345 × $(5.1)^{-1}$ × 100% = 159.5000%. This corresponds to a coverage of 3.7618 nucleotides of nuclear RNA by one polyammonium cation (spermine/spermidine ratio 0.85).

Calculation of the apparent acid dissociation constant of the human genome DNA

The intrinsic pK_a of one isolated phosphodiester of DNA is 1.29, this is the pK_a (25 °C) of dimethyl phosphate [24]. The reference *H. sapiens* genome size was taken as 3,238,442,024 bp (RefSeq assembly accession number GCF_000001405.35) [12].

Preprints (www.preprints.org) | NOT PEER-REVIEWED | Posted: 4 December 2017 doi:10.20944/preprints201701.0086.v3

The apparent (effective) $pK'_{a,HG}$ (25 °C) = 7.1849 of the haploid human genome was calculated (Figure 2A) according to the method of *Katchalsky & Gillis* [25], as based on the theoretical considerations of *Kuhn & Kuhn* [26]. The length rise of one B-DNA repeating unit (helix rise/bp) in solution (in the crystal: 0.336 nm [27,28]) was taken as: $b = 0.334 \times 10^{-7}$ cm (0.334 ± 0.01 nm [27]). The h_0 was calculated by: 0.334 nm × 3,238,442,024 = 1.08163964 m (= theoretical length of *H. sapiens* dsDNA haploid genome as linear thread). The h_v was calculated by: 0.5 × (0.334 nm + 0.5798 nm) × 3,238,442,024 = 1.47964416 m (theoretical length of half-neutralized *H. sapiens* dsDNA haploid genome as linear thread) (Figure 2A). The 0.5798 nm pitch in one relaxed (fully neutralized) dsDNA repeating unit was calculated as statistical arithmetic mean $d_{Ø}$ = 579.80 pm from the interphosphorus distance *d* (5'-*P*,5'-*P*) = 739.25 ± 14.37 pm (*d* ± s.d.; *n* = 4) in the fully ionized single-stranded hexanucleotide d(ApApApApApAp) [molecular modeling software: ACD/Chem Sketch version 12.01 with integrated ACD/3D Viewer (Advanced Chemistry Development, Inc., Toronto, Ontario, Canada), processed with Mercury 3.1 version 3.1.1 (The Cambridge Crystallographic Data Centre, Cambridge, United Kingdom)], minus the typical phosphorus–oxygen distance *d* (*P*,*O*) = 159.45 pm [29], by the formula: $d_{Ø}$ = 739.25 pm – 159.45 pm = 579.80 pm.

Calculation of the hypothetical intranuclear micro-pH mediated by single spermine occupation of human interphase euchromatin

The reference *H. sapiens* genome size was taken as 3,238,442,024 bp (RefSeq assembly accession number GCF_000001405.35) [12]. The number of base pairs for the number of protein-coding exons in *H. sapiens* genome (59,911) [12] was calculated

Preprints (www.preprints.org) | NOT PEER-REVIEWED | Posted: 4 December 2017 doi:10.20944/preprints201701.0086.v3

with the median of amino acid residues/gene (484) [12]: 59,911 × 3 bp × 484 = 86,990,772 bp (2.6862% of *H. sapiens* genome). The intrinsic pH of *H. sapiens* haploid interphase genome was calculated with the volume of a human blood lymphocyte interphase nucleus of 40.2 ± 2.0 fl (femtoliter) [9]. Because *H. sapiens* dsDNA haploid genome is to be treated as a weak acid [$pK'_{a,HG}$ (25 °C) = 7.1849], the hypothetical nuclear pH_{DNA} = 1.6642, mediated by *H. sapiens* haploid interphase genome dsDNA, can be calculated (Figure 2B). The concentration c_{DNA} was calculated as: [1 genome × (6.022140857 × 10^{23} $mol^{-1})^{-1}$] × $(40.2\ fl)^{-1}$ = 41.3069 µM. This concentration was multiplied by the number of phosphodiester moieties in dsDNA (3,238,442,024 × 2) and corrected for actively transcribed gene regions of *H. sapiens* genome (2.6862%). The four pK_a values (± s.d.) of spermine pK_{a1} = 10.86 ± 0.06, pK_{a2} = 10.05 ± 0.01, pK_{a3} = 8.82 ± 0.01, pK_{a4} = 7.95 ± 0.01 [potentiometric titration in H_2O, 25 °C, ionic strength (NaCl) 0.1] [30] give the apparent (effective) $pK'_{spermine}$ (25 °C) = 9.42 ± 0.02 (mean ± s.d.). Because the hypothetical nuclear concentration of spermine tetracation covering B-DNA is one quarter of c_{DNA}, if we assume one spermine molecule covering four base pairs (single occupation) of B-DNA [31], and correcting for actively transcribed gene regions of *H. sapiens* genome (2.6862%), the $pH_{spermine}$ = 13.1867 can be calculated (Figure 2B). Therefore, the hypothetical intranuclear micro-pH surrounding *H. sapiens* haploid interphase euchromatin when covered (single quartet occupation) by the spermine tetracation can be calculated as: $pH_{DNA/spermine}$ = 0.5 × (1.6642 + 13.1867) = 7.4255. For the diploid dsDNA genome, after completed S phase during interphase, the hypothetical micro-pH surrounding *H. sapiens* diploid interphase euchromatin when

Preprints (www.preprints.org) | NOT PEER-REVIEWED | Posted: 4 December 2017 doi:10.20944/preprints201701.0086.v3

228 covered (single quartet occupation) by the spermine tetracation is, again, $pH_{DNA/spermine}$ =
229 7.4255.
230
231 **Calculation of the theoretical intranuclear micro-pH mediated by**
232 **sperminium phosphate/cyclooctaoxygen sodium complex occupation**
233 **of human interphase euchromatin**
234 The apparent $pK'_{spermine}$ was corrected for the monohydrogen phosphate
235 complexation to get the apparent (effective) pK'_{shell} of the sperminium
236 phosphate/cyclooctaoxygen sodium complex epigenetic shell. *Ortho*-phosphoric acid
237 H_3PO_4 shows the pK_{a1} = 2.161, pK_{a2} = 7.207, and pK_{a3} = 12.325 at 25 °C [32].
238 Therefore, the $pK'_{spermine}$ is to be corrected for the monohydrogen phosphate of the
239 epigenetic shell: pK'_{shell} = [9.42 + ({[(2.161 + 7.207) × 0.5] + 12.325} × 0.5)] × 0.5 =
240 8.96225. Because the theoretical nuclear concentration of the sperminium
241 phosphate/cyclooctaoxygen sodium complex covering dsDNA is two-third of c_{DNA}, when
242 we assume one epigenetic complex molecule covering three base pairs on both strands
243 of dsDNA (double occupation), and correcting for actively transcribed gene regions of *H.*
244 *sapiens* genome (2.6862%), the pH_{shell} = 13.1708 (Figure 2B). Therefore, the theoretical
245 intranuclear micro-pH surrounding *H. sapiens* haploid interphase euchromatin when
246 covered (double triplet occupation) by the sperminium phosphate/cyclooctaoxygen
247 sodium complex can be calculated as: $pH_{DNA/shell}$ = 0.5 × (1.6642 + 13.1708) = 7.4175.
248 For the diploid dsDNA genome, after completed S phase during interphase, the
249 theoretical micro-pH surrounding *H. sapiens* diploid interphase euchromatin when

Preprints (www.preprints.org) | NOT PEER-REVIEWED | Posted: 4 December 2017 doi:10.20944/preprints201701.0086.v3

covered (double triplet occupation) by the sperminium phosphate/cyclooctaoxygen sodium complex is, again, $pH_{DNA/shell}$ = 7.4175.

Color assay for cyclo-O_8-Na^+ contained in RC – Destruction of cyclo-O_8-Na^+ by the glyphosate metabolite (aminomethyl)phosphonic acid

Stock preparations were: KI (52 mg KI in 2,000 µl H_2O) (**1**), KI + starch (52 mg KI + 18 mg starch in 2,000 µl H_2O) (**2**), **RC** + KI (34 mg **RC** + 52 mg KI in 2,000 µl H_2O) (**3**), **RC** + KI + AMPA (34 mg **RC** + 52 mg KI + 22 mg AMPA in 2,000 µl H_2O) (**4**), **RC** + KI + starch (34 mg **RC** + 52 mg KI + 18 mg starch in 2,000 µl H_2O) (**5**), **RC** + KI + starch + AMPA (34 mg **RC** + 52 mg KI + 18 mg starch + 22 mg AMPA in 2,000 µl H_2O) (**6**). The concentrations in solution were: **RC**, 16.95 mM (with cyclo-O_8-Na^+, 67.79 mM); KI, 156.63 mM; AMPA, 99.06 mM.

The stock solutions were incubated at room temperature (RT, ϑ = 14.0 °C) for 30 min, then at elevated temperature (ϑ = 25.2 °C) for 2 min, after which time the first photograph series (Figure 3) was taken. The solutions were then incubated at elevated temperature for 48 min, after which time the second photograph (Figure 3) series was taken. The solutions were further incubated at RT for 14 h. Afterwards, both **RC** + KI (**3**) and **RC** + KI + AMPA (**4**) were mixed with 1,000 µl deuterated chloroform ($CDCl_3$), and extracted by shaking. Concomitantly, **RC** + KI + starch (**5**) and **RC** + KI + starch + AMPA (**6**) were both mixed with 8 mg of solid L-ascorbic acid (concentration of L-ascorbic acid in solution 22.71 mM). The solutions were succeedingly incubated at elevated temperature for 15 min, after which time the third photograph series (Figure 3) was taken.

Preprints (www.preprints.org) | NOT PEER-REVIEWED | Posted: 4 December 2017 doi:10.20944/preprints201701.0086.v3

Control color assay for potential reduction of elemental iodine by the glyphosate metabolite (aminomethyl)phosphonic acid

Stock preparations were: blank without AMPA (1,000 µl H_2O), AMPA stock solution (34 mg AMPA in 1,000 µl H_2O), and two iodine stock solutions [each 80 mg elemental iodine in 2,000 µl 90% (*v*/*v*) aqueous ethanol]. The stock preparations were incubated at room temperature (RT, ϑ = 14.0 °C) for 15 min with occasional shaking, then at elevated temperature (ϑ = 25.2 °C) for 15 min, until the stock preparations were nearly dissolved (AMPA full, iodine not fully). Then the AMPA stock solution was injected into the first iodine stock solution (it results solution **A**), no decoloration resulted. The H_2O blank was injected into the second iodine stock solution (it results solution **B**), no decoloration resulted. The concentrations in solution were now: AMPA, 102.07 mM; iodine as I_2, 105.07 mM.

After incubation at elevated temperature for 15 min, into both solutions 1,000 µl of water were injected, crystallization of elemental iodine followed, and no decoloration resulted. The first photograph series (Figure 3) was taken after 25 min incubation at elevated temperature. After incubation at elevated temperature for 15 min, 2,000 µl of 90% (*v*/*v*) aqueous ethanol were injected in both **A** and **B**. The mixtures were shaken, the iodine dissolved to give clear deep brown solutions, and no decoloration resulted. After 5 min incubation at elevated temperature the second photograph (Figure 3) series was taken. Both **A** and **B** did not show any further change at RT during 24 h observation.

Preprints (www.preprints.org) | NOT PEER-REVIEWED | Posted: 4 December 2017 doi:10.20944/preprints201701.0086.v3

Color assay for cyclo-O_8-Na^+ contained in RC – Destruction of cyclo-O_8-Na^+ by glyphosate and ROUNDUP®

Stock preparations were: **RC** + KI + starch (34 mg **RC** + 57 mg KI + 18 mg starch in 2,000 µl H_2O) (**1**), **RC** + KI + starch + glyphosate (34 mg **RC** + 57 mg KI + 18 mg starch + 34 mg glyphosate in 2,000 µl H_2O) (**2**), **RC** + KI + starch + glyphosate-Na (34 mg **RC** + 57 mg KI + 18 mg starch + 87 mg ROUNDUP® GRAN in 2,000 µl H_2O) (**3**), **RC** + KI + glyphosate (34 mg **RC** + 57 mg KI + 34 mg glyphosate in 2,000 µl H_2O) (**4**), **RC** + KI + glyphosate-Na (34 mg **RC** + 57 mg KI + 87 mg ROUNDUP® GRAN in 2,000 µl H_2O) (**5**) [a saturated solution of 18 mg glyphosate (free acid) in 1,000 µl of H_2O showed pH 1.5 (14.0 °C)]. The concentrations in solution were: **RC**, 16.95 mM (with cyclo-O_8-Na^+, 67.79 mM); KI, 171.69 mM; glyphosate, 100.55 mM; glyphosate-Na, 108.15 mM. The stock solutions were incubated at room temperature (RT, ϑ = 14.7 °C) for 30 min, then at elevated temperature (ϑ = 25.2 °C) for 70 min, after which time the photograph series (Figure 4) was taken.

A control color assay for potential reduction of elemental iodine by glyphosate and ROUNDUP® GRAN was performed. Stock preparations were: blank without glyphosate [75 mg elemental iodine in 2,000 µl 45% (*v*/*v*) aqueous ethanol], glyphosate stock solution [52 mg glyphosate in 2,000 µl 45% (*v*/*v*) aqueous ethanol], and ROUNDUP® GRAN stock solution [124 mg ROUNDUP® GRAN in 2,000 µl 45% (*v*/*v*) aqueous ethanol]. The stock preparations were incubated at room temperature (RT, ϑ = 14.1 °C) for 45 min with occasional shaking. Then 75 mg solid elemental iodine were added to both glyphosate and ROUNDUP® GRAN stock preparation. After incubation at elevated temperature for 1.5 h, the stock preparations were nearly dissolved

Preprints (www.preprints.org) | NOT PEER-REVIEWED | Posted: 4 December 2017 doi:10.20944/preprints201701.0086.v3

(ROUNDUP® GRAN full, glyphosate and iodine not fully). Then 1,000 µl of 90% (*v*/*v*) aqueous ethanol were injected into each preparation [resulting in solution **A1** (glyphosate), **A2** (glyphosate-Na), and **B** (blank)], no decoloration resulted. The concentrations in solution were now: glyphosate, 102.52 mM; glyphosate-Na, 102.77 mM; iodine as I_2, 98.50 mM. The photograph series (Figure 4) was taken after 6 h incubation at elevated temperature, no decoloration resulted. Both **A1**, **A2**, and **B** did not show any further change at RT during 24 h observation.

A color assay for cyclo-O_8-Na^+ contained in **NC** was accordingly performed. The preparation was: **NC** + KI + starch (25 mg **NC** + 43 mg KI + 18 mg starch in 1,000 µl H_2O). The concentrations in solution were: **NC**, 18.25 mM (with cyclo-O_8-Na^+, 18.25 mM); KI, 259.04 mM. The preparation was incubated at elevated temperature for 10 h, after which time the first photograph (Figure 4) series was taken. The preparation was further incubated at room temperature (RT, ϑ = 13.7 °C) for 40 h, after which time the second photograph series (Figure 4) was taken.

Enzyme assay of the glyphosate metabolite (aminomethyl)phosphonic acid with human mitochondrial γ-aminobutyric acid transaminase

Recombinant human (16p13.2) mitochondrial 4-aminobutyrate aminotransferase (ABAT) (E.C. 2.6.1.19), mature full length protein aa 29–500 with N-terminal His-SUMO-tag and C-terminal Myc-tag, was purchased from MyBioSource, Inc. (San Diego, CA, USA). The sequence (472 aa) is:
SQAAAKVDVEFDYDGPLMKTEVPGPRSQELMKQLNIIQNAEAVHFFCNYEESRGNYLV

Preprints (www.preprints.org) | NOT PEER-REVIEWED | Posted: 4 December 2017 doi:10.20944/preprints201701.0086.v3

DVDGNRMLDLYSQISSVPIGYSHPALLKLIQQPQNASMFVNRPALGILPPENFVEKLRQ SLLSVAPKGMSQLITMACGSCSNENALKTIFMWYRSKERGQRGFSQEELETCMINQA PGCPDYSILSFMGAFHGRTMGCLATTHSKAIHKIDIPSFDWPIAPFPRLKYPLEEFVKEN QQEEARCLEEVEDLIVKYRKKKKTVAGIIVEPIQSEGGDNHASDDFFRKLRDIARKHGC AFLVDEVQTGGGCTGKFWAHEHWGLDDPADVMTFS**K**KMMTGGFFHKEEFRPNAPY RIFNTWLGDPSKNLLLAEVINIIKREDLLNNAAHAGKALLTGLLDLQARYPQFISRVRGR GTFCSFDTPDDSIRNKLILIARNKGVVLGGCGDKSIRFRPTLVFRDHHAHLFLNIFSDILA DFK (PLP-binding K_{357} active site in bold). The 500 aa ABAT precursor protein (NCBI Reference Sequence NP_000654.2) additionally bears the N-terminal peptide 1–28. The mature ABAT (aa 29–500, 53.27 kDa) is responsible for the catabolism of γ-aminobutyric acid (GABA), an important, mostly inhibitory neurotransmitter in the central nervous system, into succinic semialdehyde. The active enzyme is a homodimer of 53 kDa subunits, each condensed to one pyridoxal 5'-phosphate (PLP). The human ABAT deficiency phenotype includes psychomotor retardation, hypotonia, hyperreflexia, lethargy, refractory seizures, and electroencephalographic (EEG) abnormalities.

To investigate whether AMPA is a substrate for human mitochondrial GABA transaminase, experiments were performed with commercially available recombinant human GABA transaminase according to the procedure of *Schor et al.* [33] with some modifications. Incubations with 500 nmol AMPA, in an assay volume of 120 µl did not show activity of GABA transaminase towards AMPA, while the control assay using 500 nmol ^{15}N-GABA as substrate did result in the formation of the expected enzyme product. Subsequent inhibition experiments, with co-incubations of fixed amounts (500 nmol) of ^{15}N-GABA with increasing amounts of AMPA (0–2000 nmol), revealed that

Preprints (www.preprints.org) | NOT PEER-REVIEWED | Posted: 4 December 2017 doi:10.20944/preprints201701.0086.v3

AMPA did not act as an inhibitor of the GABA transaminase-catalysed reaction of ^{15}N-GABA to succinic semialdehyde. These combined results strongly suggest that AMPA is not a substrate for human GABA transaminase.

Enzyme assay of the glyphosate metabolite (aminomethyl)phosphonic acid with human wild-type alanine:glyoxylate aminotransferase

Recombinant human alanine:glyoxylate aminotransferase was expressed in *E. coli* and purified as described [34]. The enzyme at 5 µM concentration was incubated with 100 mM AMPA at 25 °C in 100 mM potassium phosphate buffer pH 7.4. At various times (1, 2, 5, 22 h), aliquots were withdrawn and the reaction was stopped by adding trichloroacetic acid 10% (*v*/*v*). The total amount of PLP and pyridoxamine 5'-phosphate (PMP) was determined by HPLC analysis as previously described (Figure 5A) [35].

Results

Cyclooctaoxygen

The chemical element oxygen exists in eight well-characterized allotropic modifications, dioxygen (O_2), ozone (O_3), and the solid α-, β-, γ-, δ-, ε- and ζ-oxygen phases [36]. The γ-, β- and α-phases exist at ambient pressure and low temperature [5,36,37]. At ambient temperature under pressure of 5.4 GPa oxygen solidifies into the β-phase, then at 9.6 GPa into the orthorhombic 'orange' δ-phase, and, successively, at 10 GPa into the monoclinic 'dark red' ε-phase. Above 96 GPa ε-oxygen is transformed

Preprints (www.preprints.org) | NOT PEER-REVIEWED | Posted: 4 December 2017 doi:10.20944/preprints201701.0086.v3

into the metallic ζ-phase which exhibits superconductivity [5,36,37]. The 'red' ε-phase revealed the structure of two combined tetroxetane (cyclo-O_4) rings, giving rise to rhombohedral O_8 clusters [37]. In 1990 a ninth allotropic modification of oxygen was theoretically predicted [38], the cyclooctaoxygen (cyclo-O_8, octoxocane) (Figure 6A) [36,38], assumed to exist in analogy to the common modification of elemental sulfur, cyclooctasulfur (cyclo-S_8, octathiocane) [38]. We reported [5] the (biomimetic) synthesis, isolation, chemical characterization, biochemical and epigenetic significance of cyclo-O_8 in form of its sodium crown complex, (octoxocane-κ^4O^1,O^3,O^5,O^7)sodium(1+) or cyclo-O_8-Na^+ (Figure 6B) [5].

The isolation of two cyclooctaoxygen complexes NC and dNC

In an endeavor to gain new antiviral substances, the reported reaction [39] of the RNA nucleoside cytidine with ninhydrin on reflux was re-examined. Instead of cytidine, cytidine hydrochloride (cytidine × HCl) was utilized. The reported reaction [39] did not proceed, instead a crystalline material **NC** could be isolated which gave not the elemental analysis of cytidine × HCl. It could be substantiated that **NC** contained an inert material not being salt (NaCl), since the *Fourier* transform infrared (FT–IR) spectrum of **NC** differed from that of cytidine × HCl. According to elemental analysis this inert material could account for one O_2 and a quarter of NaCl *pro* one cytidine × HCl. In consequence, the formula was multiplied fourfold and this resulted in an oxygen 8-ring, cyclo-O_8 (Figure 6A), coordinated to one Na^+ (Figure 6B). The interpretation of the electrospray ionization mass spectrometry (ESI–MS) spectrum of **NC** actually proved the inclusion of cyclo-O_8-Na^+ in **NC**. Since in the proton nuclear magnetic resonance

Preprints (www.preprints.org) | NOT PEER-REVIEWED | Posted: 4 December 2017 doi:10.20944/preprints201701.0086.v3

(^{1}H-NMR) spectrum of **NC**, in comparison to the ^{1}H-NMR reference spectrum of cytidine × HCl, the differentially affected resonances were the 4-NH_2, the 3-NH^+, and the H-5 protons of the protonated cytidine, it was assumed [5] that the points of coordination between cyclo-O_8-Na^+ and cytidine × HCl are the two 4-NH_2 hydrogens and one non-Na^+-coordinated (free) oxygen of cyclo-O_8-Na^+. Consequently, a formula for **NC** was elaborated: cytidine hydrochloride – aqua(chloro)(octoxocane-κ^4O^1,O^3,O^5,O^7)sodium (4:1) (Figure 7A) [5].

The new ninhydrin reaction was in turn applied on 2'-deoxycytidine hydrochloride (2'-deoxycytidine × HCl). A crystalline material **dNC** could be isolated which gave not the elemental analysis of 2'-deoxycytidine × HCl. The FT–IR spectrum of **dNC** differed from that of 2'-deoxycytidine × HCl. The interpretation of the ESI–MS spectrum of **dNC** proved the inclusion of cyclo-O_8-Na^+ in **dNC**. In analogy to **NC**, supported by ^{1}H-NMR spectroscopy of **dNC**, a formula for **dNC** could be constructed: 2'-deoxycytidine hydrochloride – aqua(chloro)(octoxocane-κ^4O^1,O^3,O^5,O^7)sodium (2:1) (Figure 7B) [5].

Catalase assay of NC and *Candida utilis* RNA – Biomimetic synthesis of RC – Structure proof for cyclooctaoxygen

It was questioned if cyclo-O_8-Na^+ could be produced in biomimetic reactions, and it was considered that in the two ninhydrin reactions atmospheric oxygen was the source of the oxygen atoms in cyclo-O_8. My interest concentrated on oxygen formation by possible catalase effects under physiological conditions. The catalase effect is the disproportionation of dihydrogen peroxide (H_2O_2) into oxygen and water: 2 H_2O_2 → O_2 +

Preprints (www.preprints.org) | NOT PEER-REVIEWED | Posted: 4 December 2017 doi:10.20944/preprints201701.0086.v3

2 H_2O. As a catalyst RNA was selected, since RNA can exhibit enzymatic (ribozyme) activities *in vivo* [40,41]. The selected eukaryotic RNA was *Candida utilis* anamorph yeast low-molecular weight RNA. This RNA consists of transfer RNAs (tRNAs) and the *C. utilis* 5S ribosomal RNA (rRNA) [5]. As a result it was discovered that **NC** catalysed oxygen formation from H_2O_2 (catalase effect) weakly in presence of $NaHCO_3$, and strongly in presence of both *C. utilis* RNA and $NaHCO_3$ [5]. Interestingly, **NC** could be fully substituted by cytidine × HCl. Multiple controls assured that oxygen neither was produced spontaneously, nor from any other relevant combination of the utilized reagents. Taken together, the nucleoside cytidine, not cyclo-O_8-Na^+, was responsible for the catalase activity expressed in presence of H_2O_2 and *C. utilis* RNA under biomimetic conditions. It was decided to exactly scale-up (21-fold) the catalase assay protocol starting with cytidine × HCl and *C. utilis* RNA to detect any cyclo-O_8-Na^+ formation under biomimetic conditions. From this preparation a cyclo-O_8-Na^+-containing crystalline material **RC** could be isolated which gave not the elemental analysis of cytidine × HCl. If the *C. utilis* RNA was omitted, no product **RC** could be isolated, only cytidine × HCl. Based on ^{1}H-NMR spectroscopy and FT–IR spectroscopy of **RC**, a formula for **RC** could be constructed: cytidine hydrochloride – μ-chloro(μ-hydroxy)bis(octoxocane-κ^4O^1,O^3,O^5,O^7)disodium (1:2) (Figure 7C) [5].

Final structure proof for the existence of cyclo-O_8 was obtained from the ESI–MS of **RC** (Figure 8). Cluster cations of heptoxazocan-8-ium – octoxocane – $Na^{35}Cl$ (1:2:*m*) (*m* = 0–6) were observed, together with characteristic +2 isotope peaks resulting from substitution of one ^{37}Cl for ^{35}Cl (*m* = 1–6), and together with –2 peaks of heptoxazocan-8-iumyl – octoxocane (1:2) cluster radical cations (*m* = 0–6) (Figure 8). Clusters of

Preprints (www.preprints.org) | NOT PEER-REVIEWED | Posted: 4 December 2017 doi:10.20944/preprints201701.0086.v3

455 $[(\text{cytidine})_2 + \text{Na} + (\text{NaCl})_n]^+$ (n = 0–5) were also observed (Figure 8). Structure proving
456 was the missing of a +2 peak for m = 0 (Figure 8, inset), indicating that any NaCl is
457 absent in this radical cation m/z 383.9907. The nitrogen insertion into cyclo-O_8 to give
458 heptoxazocane (HNO_7) resulted from mass spectrometric generation of ammonia NH_3
459 from cytidine ($O_8 + NH_3 \rightarrow HNO_7 + H_2O$).

460

461 ## Binding of NC to *Candida utilis* RNA

462 In view of the biomimetic generation of the cyclo-O_8-Na^+-containing coordination
463 complex **RC**, the question arose if cyclo-O_8-Na^+ could bind to nucleic acids, because of
464 the mere electrostatic attraction of the cyclo-O_8-Na^+ cation towards the negatively
465 charged phosphate backbone of RNA and DNA. For this purpose thin-layer
466 chromatographic mobility shift assays [42] were applied on specific nucleic acids and
467 the cyclo-O_8-Na^+ contained in **NC**. Firstly, the affinity of the cyclo-O_8-Na^+ towards *C.*
468 *utilis* low-molecular weight RNA was investigated [5]. It was found that the cyclo-O_8-Na^+
469 contained in **NC** retained the chromatographic shift of *C. utilis* 5S rRNA, but not the
470 chromatographic shift of *C. utilis* tRNAs. Interestingly, since work conditions were not
471 human skin ribonuclease (RNase)-free, the RNase A digestion products of *C. utilis* 5S
472 rRNA were separated chromatographically [5]. These dinucleotide 2',3'-cyclic
473 phosphates (products of RNase A digestion) result from human skin RNase 7-mediated
474 digestion of *C. utilis* 5S rRNA [5]. The structures of these dinucleotides can be deduced,
475 since RNase 7 belongs to the RNase A superfamily [5]. The cyclo-O_8-Na^+ contained in
476 **NC** bound strongly to these dinucleotide 2',3'-cyclic phosphates, since their
477 chromatographic shifts were significantly retarded. Controls were included to

Preprints (www.preprints.org) | NOT PEER-REVIEWED | Posted: 4 December 2017 doi:10.20944/preprints201701.0086.v3

differentiate the sole binding of cytidine × HCl to the RNA targets by *Watson–Crick* base pairing [43] from the indicative cyclo-O_8-Na^+ *plus* cytidine × HCl binding to the RNA targets.

Binding of NC to salmon testes single-stranded DNA and spermine phosphate

Accordingly, the affinity of the cyclo-O_8-Na^+ contained in **NC** towards salmon testes single-stranded deoxyribonucleic acid [ssDNA, generated by sonication of salmon genomic double-stranded DNA (dsDNA); extracted after sonication by phenol–chloroform method and precipitated with ethanol; the sonication shears the genomic dsDNA to produce ssDNA fragments in the range of 587 to 831 bp] was investigated (Figure 9) [5]. It was found that the cyclo-O_8-Na^+ contained in **NC** retained the chromatographic shift of cytidine × HCl complexed to ssDNA (Figure 9). As control served cytidine × HCl complexed to ssDNA. The affinity of the cyclo-O_8-Na^+ contained in **NC** towards salmon testes ssDNA in absence and presence of spermine × 1 ⅓ (sodium dihydrogen phosphate) × 9 H_2O was investigated [5]. It was found that the spermine × 1 ⅓ (sodium dihydrogen phosphate) × 9 H_2O changed the chromatographic shift of the cytidine × HCl in **NC**-complexed ssDNA. As controls served cytidine × HCl complexed to ssDNA in absence and presence of cyclo-O_8-Na^+, and cytidine × HCl complexed to ssDNA in presence of spermine × 1 ⅓ (sodium dihydrogen phosphate) × 9 H_2O [5]. Taken together, cyclo-O_8-Na^+ contained in **NC** had the ability to bind to RNA dinucleotide 2',3'-cyclic phosphates, eukaryotic 5S rRNA, eukaryotic ssDNA, and to construct a ternary complex with spermine phosphate and eukaryotic ssDNA.

Preprints (www.preprints.org) | NOT PEER-REVIEWED | Posted: 4 December 2017 doi:10.20944/preprints201701.0086.v3

501

502 *In vitro* biological effects of NC and dNC on cultured mammalian cells

503 The *in vitro* biological effects of **NC** and **dNC** on the growth of cultured cells,
504 freshly explanted human primary (human peripheral blood mononuclear cells, PBM
505 cells), immortalized T-lymphoblastic (CCRF–CEM) and monkey kidney normal epithelial
506 (Vero), were investigated [5]. **NC** and **dNC** were non-toxic to PBM cells, but stimulated
507 the growth of CCRF–CEM cells. This pointed to a catalase effect exerted by **NC** and
508 **dNC**, since CCRF–CEM cells are extremely sensitive to H_2O_2 [5], and scavenging of
509 H_2O_2 by 'catalase factors' is CCRF–CEM cell growth rate-limiting [5]. Since **NC** was
510 more active as a growth stimulant for CCRF–CEM cells than **dNC**, the responsible
511 'catalase factors' should be the nucleoside hydrochlorides, not the equimolar cyclo-O_8-
512 Na^+-content in **NC** and **dNC**. **NC** and **dNC** exhibited no significant *in vitro* antiviral
513 activities against the *retro*-transcribing human immunodeficiency type 1 and hepatitis B
514 viruses (HIV-1 strain LAI and HBV subtype ayw) [5]. **NC** showed no significant *in vitro*
515 inhibiting activity versus the replication of influenza A (H1N1 and H5N1) and
516 chikungunya (strain S-27) viruses, and no significant *in vitro* inhibiting activity on Middle
517 East respiratory syndrome (MERS) coronavirus (MERS-CoV strain Erasmus Medical
518 Center/2012) replication [5]. In summary, cyclo-O_8-Na^+ is, contrary to expectation,
519 essentially non-toxic to human cells, and cytidine in conjunction with RNA acts as a
520 catalyst in producing cyclo-O_8-Na^+ from ubiquitous [5] H_2O_2 through a catalase reaction
521 in cultured human cells.

522

Preprints (www.preprints.org) | NOT PEER-REVIEWED | Posted: 4 December 2017 doi:10.20944/preprints201701.0086.v3

Color assay for cyclo-O_8-Na^+ contained in RC – Destruction of cyclo-O_8-Na^+ by the glyphosate metabolite (aminomethyl)phosphonic acid

The cyclo-O_8-Na^+ complex [μ-chloro(μ-hydroxy)bis(octoxocane-κ^4O^1,O^3,O^5,O^7)disodium] contained in **RC** (4 mol cyclo-O_8-Na^+ *pro* mol cytidine × HCl) reacted with potassium iodide and potato starch to an intensely colored (reddish violet) [(cyclo-O_8-Na^+)$_2$(I_4^{2-})]–amylose complex [**RC** + KI + starch (**5**)] (Figure 3) which was destroyed by the glyphosate metabolite (aminomethyl)phosphonic acid (AMPA) [**RC** + KI + starch + AMPA (**6**)]. The nature of this complex is based on the starch-catalysed formation of tetraiodide I_4^{2-} [(I–I–I–I)$^{2-}$], which is known to be of ruby red color in crystalline form [44], was frequently observed in crystals [45], and was theoretically predicted to exist in solution [46]. The tetraiodide I_4^{2-} is in turn complexed to cyclo-O_8-Na^+ and inserted into the amylose helix (Figure 10A and 10B). Multiple controls excluded that the [(cyclo-O_8-Na^+)$_2$(I_4^{2-})]–amylose complex is formed (i) in blanks [KI (**1**), and KI + starch (**2**)], (ii) without starch [**RC** + KI (**3**)], and (iii) from AMPA and **RC** + KI [**RC** + KI + AMPA (**4**)] (Figure 3). That the reddish violet complex involved triiodide I_3^- [(I–I–I)$^-$] or pentaiodide I_5^- [(I–I–I–I–I)$^-$] anions could be excluded by the observed color. Triiodide I_3^- is deep brown [47] and pentaiodide I_5^- is deep blue in color [48]. Pentaiodide I_5^- is also deep blue in the well-known complex with starch [49]. Furthermore, the [(cyclo-O_8-Na^+)$_2$(I_4^{2-})]–amylose complex was (i) reduced (decolorized) by L-ascorbic acid (vitamin C), and (ii) the residual color after AMPA-catalysed destruction of cyclo-O_8 was pale pink (rosé) in color, not intense blue. This proved that (i) the reddish violet complex contained reducible iodine units, and (ii) did not contain the reducible iodine units as triiodide, pentaiodide and/or other higher polyiodides [50].

Preprints (www.preprints.org) | NOT PEER-REVIEWED | Posted: 4 December 2017 doi:10.20944/preprints201701.0086.v3

Without starch no [(cyclo-O_8-Na^+)$_2$(I_4^{2-})] and/or iodine was formed, as was proved by deuterated chloroform ($CDCl_3$) extraction of the incubated **RC** + KI (**3**) and **RC** + KI + AMPA (**4**) solutions (Figure 3). Therefore, the iodine in tetraiodide I_4^{2-} must have being formed by starch catalysis.

A logically deduced catalytic 'rolling-circle' mechanism for the AMPA-catalysed degradation of cyclo-O_8 is hence proposed (Figure 10C). AMPA exhibits three acid dissociation constants: pK_{a1} = 0.9 (phosphonic acid, 1st), pK_{a2} = 5.6 (phosphonic acid, 2nd), pK_{a3} = 10.2 (primary ammonium R–NH_3^+) [51]. Therefore, AMPA is fully (zwitter)ionized at physiological pH 7.4. One anionic oxygen of the phosphonate group binds to the sodium cation in cyclo-O_8-Na^+, the other anionic phosphonate oxygen splits the cycloocytooxygen ring creating a phosphonate-esterified nonaoxidanide which is stabilized by ionic binding to the primary ammonium cation of AMPA. The phosphonate-esterified nonaoxidanide eliminates four oxygen O_2 molecules by a 'rolling-circle' cascade, in reversal of the proposed [5] synthesis of cyclooctaoxygen, yielding AMPA and Na^+. This would be clearly a catalytic mechanism, since AMPA is regenerated in the catalytic cycle. Hence AMPA is able to destroy many cyclo-O_8-Na^+ complexes without being consumed itself.

To exclude that the destruction of cyclo-O_8-Na^+ by AMPA is an artifact, it was tested if AMPA reduces (decolorizes) iodine in near equimolar mixture (Figure 3). In all variations tested, including a blank control, AMPA was not oxidized by iodine, and, in turn, did not reduce (decolorize) iodine molecules. Therefore, the AMPA-catalysed destruction of cyclo-O_8 was selective, and not a mere reduction of the tetraiodide I_4^{2-} [(I–I–I–I)$^{2-}$]-contained iodine unit in the [(cyclo-O_8-Na^+)$_2$(I_4^{2-})]–amylose complex.

Preprints (www.preprints.org) | NOT PEER-REVIEWED | Posted: 4 December 2017 doi:10.20944/preprints201701.0086.v3

569

570 Color assay for cyclo-O_8-Na^+ contained in RC – Destruction of cyclo-
571 O_8-Na^+ by glyphosate and ROUNDUP®

572 The developed color assay was applied onto the free acid of glyphosate and the
573 monosodium salt of glyphosate contained in ROUNDUP® GRAN granules. The colored
574 [(cyclo-O_8-Na^+)$_2$(I_4^{2-})]–amylose complex [**RC** + KI + starch (**1**)] (Figure 4) was destroyed
575 by glyphosate [**RC** + KI + starch + glyphosate (**2**)] and ROUNDUP® GRAN [**RC** + KI +
576 starch + glyphosate-Na (**3**)]. Without starch no [(cyclo-O_8-Na^+)$_2$(I_4^{2-})] and/or other color
577 complex was formed, as was proved by the controls **RC** + KI + glyphosate (**4**) and **RC** +
578 KI + glyphosate-Na (**5**) (Figure 4). The **RC** + KI + starch + glyphosate (**2**) solution was
579 colored yellow by the strong acid glyphosate (Figure 4), through H^+ action onto starch
580 producing the characteristic yellow dextrins [52]. Glyphosate exhibits four acid
581 dissociation constants: pK_{a1} = 0.78 (phosphonic acid, 1st), pK_{a2} = 2.29 (carboxylic acid),
582 pK_{a3} = 5.96 (phosphonic acid, 2nd), pK_{a4} = 10.98 (primary ammonium R–NH_3^+) [51].
583 Therefore, glyphosate (free acid) represents a strong acid.

584 A logically deduced catalytic 'rolling-circle' mechanism for the glyphosate-
585 catalysed degradation of cyclo-O_8 is hence proposed (Figure 11). One anionic oxygen
586 of the phosphonate group binds to the sodium cation in cyclo-O_8-Na^+, the other anionic
587 phosphonate oxygen splits the cycloocytooxygen ring creating a phosphonate-esterified
588 nonaoxidanide which is stabilized by ionic binding to the secondary ammonium cation of
589 glyphosate. The phosphonate-esterified nonaoxidanide eliminates four oxygen O_2
590 molecules by a 'rolling-circle' cascade, yielding glyphosate and Na^+ in a catalytic

Preprints (www.preprints.org) | NOT PEER-REVIEWED | Posted: 4 December 2017 doi:10.20944/preprints201701.0086.v3

mechanism. Glyphosate is regenerated in the catalytic cycle. Glyphosate is able to destroy many cyclo-O_8-Na^+ complexes without being consumed itself.

To exclude that the destruction of cyclo-O_8-Na^+ by glyphosate is an artifact, it was tested if glyphosate, or glyphosate-Na, reduces (decolorizes) iodine in near equimolar mixture (Figure 4). Glyphosate was not oxidized by iodine, and, in turn, did not reduce (decolorize) iodine molecules. Therefore, the glyphosate-catalysed destruction of cyclo-O_8 was selective. To confirm the general nature of the color assay, it was extended to the cyclo-O_8-Na^+ contained in **NC** (1 mol cyclo-O_8-Na^+ *pro* 4 mol cytidine × HCl) [5]. The reddish violet [(cyclo-O_8-Na^+)$_2$(I_4^{2-})]–amylose complex was indeed formed from **NC** (Figure 4), but much more slowly (> 10 h) than from **RC**.

Enzymatic investigations with the glyphosate metabolite (aminomethyl)phosphonic acid

AMPA was tested for being accepted as an enzymatic substrate for human mitochondrial γ-aminobutyric acid transaminase (ABAT) [33], and wild-type human liver peroxisomal alanine:glyoxylate aminotransferase (AGT) [53]. Both enzymes were selected because of the chemical analogy between AMPA and β-alanine/L-alanine. ABAT represents also a β-alanine transaminase [33]. Data obtained with human AGT indicate that the enzyme is barely able to catalyse the half-transamination of AMPA, with a rate of k_{cat} = – 0.0108 ± 0.0009 µM PLP/h/µM AGT consumed, or k_{cat} = – 0.0104 ± 0.0009 µM PMP/h/µM AGT formed (Figure 5A), respectively (PLP, pyridoxal 5'-phosphate; PMP, pyridoxamine 5'-phosphate). This value is approximately 16.2 million-

Preprints (www.preprints.org) | NOT PEER-REVIEWED | Posted: 4 December 2017 doi:10.20944/preprints201701.0086.v3

fold lower than that of the physiological transamination of L-alanine (human wild-type AGT: k_{cat} = 45 ± 2 s^{-1}; k_{cat} = 162,000 h^{-1}) [53].

Discussion

One reason why the cyclooctaoxygen sodium-bridged spermine phosphate epigenetic shell of *in vivo* DNA was overlooked until now should be its destruction during DNA purification by the classical phenol extraction method of *Schuster*, *Schramm* & *Zillig* [54]. This original phenol extraction, although variously modified for nowadays use [55], consistently precipitates the spermine as sperminediium (terminal NH_3^+) di(phenolate) at pH 7.9–8.0 [55], since the pK_a value of phenol is 9.97 [potentiometric titration in H_2O, 25 °C, ionic strength (NaCl) 0.1] [56], and the four pK_a values of spermine are: pK_{a1} = 10.86 (terminal [57] NH_3^+), pK_{a2} = 10.05 (terminal NH_3^+), pK_{a3} = 8.82 (inner [57] NH_2^+), pK_{a4} = 7.95 (inner NH_2^+) [potentiometric titration in H_2O, 25 °C, ionic strength (NaCl) 0.1] [30]. The cyclo-O_8-Na^+ could react with alkaline (pH 7.9–8.0) buffered phenol [55] to disodium rhodizonate ($C_6Na_2O_6$), a known [58] oxidation product of *p*-benzoquinone, which in turn is an oxidation product of phenol [59]. Regardless of the chemical details, the commercial salmon sperm DNA (utilized in [5]) and calf thymus DNA preparations are devoid of cyclo-O_8-Na^+ and spermine phosphate complexation, since the methods utilized for calf thymus [60] and salmon sperm [61] sodium deoxyribonucleate preparation (treatment with sodium dodecyl sulfate [60], high salt (NaCl) treatment [60,61], repeated ethanol precipitation [60,61]) certainly remove the cyclooctaoxygen sodium-bridged spermine phosphate epigenetic shell.

Preprints (www.preprints.org) | NOT PEER-REVIEWED | Posted: 4 December 2017 doi:10.20944/preprints201701.0086.v3

My findings have important consequences for the epigenetics [62] of eukaryotic *in vivo* DNA. I suggested [5] a model for a first epigenetic shell of *in vivo* DNA (Figure 12), based on the observed complexation of cyclo-O_8-Na^+ and spermine phosphate to ssDNA. In my model (Figure 12A) the phosphate backbone of ssDNA binds one cyclo-O_8-Na^+ *pro* three nucleotides, and this binary complex binds one spermine monophosphate to form a ternary epigenetic core of DNA. The monohydrogen phosphate bridges the cyclo-O_8-Na^+ with the sperminium cation, and the cyclo-O_8-Na^+ has an inverted alternating orientation (Figure 12A). Interestingly, the sperminium tetracation cannot bind alone to DNA in this model, since the distances [d (N^1,N^4) = 490 pm; d (N^4,N^9) = 620 pm; d (N^1,N^{12}) = 1,600 pm] between the four ammonium nitrogens do not fit the intrastrand phosphate–phosphate distance of dsDNA (B-DNA: $d_{\varnothing}$ = 700 pm [63,64]; A-DNA: $d_{\varnothing}$ = 590–600 pm [64–67]; Z-DNA: $d_{\varnothing}$ = 590 pm (step pCp), $d_{\varnothing}$ = 600 pm (step pGp) [67]). Therefore, it is quite remarkable that in my model for the first epigenetic shell of *in vivo* DNA (Figure 12A) a repeating unit is formed from cyclo-O_8-Na^+ and spermine phosphate that perfectly fits both the triplet nature of the genetic code [68] and the repeating distance of the phosphate anion backbone of DNA.

Evidence for the correctness of this model results from the published investigation of spermine distribution in bovine lymphocytes [11]. The theoretical intracellular concentration of the sperminium phosphate/cyclo-O_8-Na^+ complex required to cover all triplets of the dsDNA genome in a blood lymphocyte of *Bos taurus* was calculated as 13.81 mM (see Methods) [5]. The actual concentration of spermine was measured as 1.57 ± 0.12 (mM ± s.d.) [11]. Therefore, the genomic dsDNA coverage of *B. taurus* genome can be calculated as 2.62 ± 0.50 (% ± s.d.) [5], since one unit of

Preprints (www.preprints.org) | NOT PEER-REVIEWED | Posted: 4 December 2017 doi:10.20944/preprints201701.0086.v3

sperminium phosphate/cyclo-O_8-Na^+ complex is assumed to cover three nucleotides. A good correlation was obtained when this value was compared to the proportion of protein-coding exons in *B. taurus* genome which was calculated as 2.58%. For comparison, the human genome contains 2.69% protein-coding exons. This pointed to complete coverage of actively transcribed gene regions in *B. taurus* interphase genome by the sperminium phosphate/cyclo-O_8-Na^+ complex. Since spermine binds more strongly to GC-rich dsDNA (pBR322 plasmid) [11], it can be assumed that the sperminium phosphate/cyclo-O_8-Na^+ complex binds preferentially to epigenetic, non-5-methylated CpG island hotspots [5] and is involved in epigenetic gene regulation [5].

In view of the important findings of *Kirmes et al.* [4] I was not aware of in 2015, that an interaction of eukaryotic chromatin DNA structure with atmospheric oxygen partial pressure takes place, I have to correct now previous postulations [5]. I concluded that the cyclooctaoxygen sodium-bridged spermine phosphate epigenetic shell is confined to both interphase relaxed euchromatin and mitotic condensed chromatin [5]. Since, under switching to hypoxic conditions eukaryotic cell chromatin gets highly condensed [4], accompanied by redistribution of the polyamine pool to the nucleus [4], the cyclooctaoxygen sodium-bridged spermine phosphate epigenetic shell can only be restricted to actively transcribed gene regions of eukaryotic ‘open’ euchromatin, excluding occupation of condensed chromatin. Hypoxia should largely prevent metabolic formation of cyclooctaoxygen. Both under hypoxic conditions and in the metaphase of mitosis, where spermine synthesis is highest [69], coincident with an extraordinary high condensation grade (15,000–20,000-fold) of metaphase chromatin [70], no or few cyclooctaoxygen should be involved in covering the highly condensed

Preprints (www.preprints.org) | NOT PEER-REVIEWED | Posted: 4 December 2017 doi:10.20944/preprints201701.0086.v3

chromatin DNA. Here no or few discrimination between eu- and heterochromatin is made, and all eukaryotic chromatin DNA is complexed with spermine tetracation and spermidine trication (and, at small proportions, with putrescine and cadaverine dications).

This is supported by the published concentration of spermine in the metaphase chromatin of eukaryotic HeLa S3 cells [15]. The content of spermine in HeLa S3 cell metaphase chromatin was calculated as 135.9 ± 16.1 pmol spermine/82.84 zmol dsDNA, and 116.1 ± 11.8 pmol spermidine/82.84 zmol dsDNA [5,15]. This corresponds to 1.64×10^9 molecules spermine *pro* one HeLa S3 cell dsDNA genome, and 1.40×10^9 molecules spermidine *pro* one HeLa S3 cell dsDNA genome. Since one spermine molecule is assumed to cover six base pairs (in the pure spermine form of A-DNA duplex [16] and Z-DNA duplex [17]), and one spermidine molecule is assumed to cover six base pairs (in the pure spermidine form of Z-DNA duplex [18,19]), this corresponds to a genomic coverage of 50.4% by the spermine tetracation, and of 43.0% by the spermidine trication. This accounts for 93.4% polyamine occupation of HeLa S3 cell dsDNA highly condensed metaphase chromatin by spermine and spermidine, calculated for six base pairs/polyamine unit. As one spermine molecule, in one special occasion, was found to cover four base pairs of an unique B-DNA [31], these values could be anticipated as being lower, since chromosomal DNA is predominantly in the B-DNA form.

Indirect control for this *in vitro* result is the published elemental phosphorus content [*w* (P) in mmol/kg dry weight] in female *Mus musculus* strain C3H/HeJ cryptal enterocytic mitotic (late anaphase/early telophase) chromatin [20]. The obtained *in vivo*

Preprints (www.preprints.org) | NOT PEER-REVIEWED | Posted: 4 December 2017 doi:10.20944/preprints201701.0086.v3

value corresponds to a genomic dsDNA coverage (calculated for 6 bp/polyamine) of 102.1% (100% coverage is 5.88 bp/polyamine), and a nuclear RNA coverage (calculated for 6 nucleotides/polyamine) of 159.5%, by the spermine tetracation and spermidine trication (spermine/spermidine ratio 0.85). This strongly points to a function of polyamine occupation for nuclear RNA, assuming 100% coverage as 3.76 nucleotides/polyamine molecule. These results, both for dsDNA and nuclear RNA [hnRNA with pre-mRNAs, snRNA, snoRNA, RNase P, RNase MRP, various ncRNAs (lncRNA) and other nuclear RNAs] [71], are a logic consequence of the maximal condensation grade peaking in late anaphase/early telophase mammalian chromatin [72].

In summary, this reflects the high mitotic chromatin condensation grade and is confirming the results with hypoxia-induced chromatin condensation under coinciding polyamine pool nuclear translocation [4]. Interestingly, spermine and spermidine induced B-DNA to Z-DNA transition at epigenetic, non-5-methylated CpG island hotspots of prokaryotic plasmid DNA (pBR322 derivative) [73], but, in contrast, stabilized and condensed prokaryotic chromosomal B-DNA [74]. Z-DNA was found to be formed at CpG island transcriptional hotspots [75,76]. Regions near the transcription start site frequently contain sequence motifs favorable for forming Z-DNA, and formation of Z-DNA near the promoter region stimulates transcription [76]. All these observations point to the correctness of my model that the cyclooctaoxygen sodium-bridged spermine phosphate epigenetic shell is restricted to actively transcribed ‘hot spot’ gene regions of eukaryotic ‘open’ euchromatin. Importantly, this epigenetic shell of eukaryotic ‘open’ euchromatin covers each strand of dsDNA separately, one at the positive strand, one at

Preprints (www.preprints.org) | NOT PEER-REVIEWED | Posted: 4 December 2017 doi:10.20944/preprints201701.0086.v3

728 the negative strand (double occupation), whereas the highly condensed dsDNA
729 structures bind one polyamine molecule directly at the double strand (single occupation)
730 [16–19,31].

731 This is substantiated by the precise calculation of the apparent acid dissociation
732 constant of the human genome DNA. The apparent (effective) $pK'_{a,HG}$ (25 °C) = 7.18 of
733 the haploid human genome was calculated (Figure 2A) according to the method of
734 *Katchalsky & Gillis* [25], as based on the theoretical considerations of *Kuhn & Kuhn* [26].
735 The hypothetical intranuclear pH_{DNA} = 1.66, mediated by *H. sapiens* haploid interphase
736 genome dsDNA without any neutralizing shell, can be calculated (Figure 2B). Assuming
737 one spermine molecule covering four base pairs (single occupation) of B-DNA [31], and
738 correcting for actively transcribed gene regions of *H. sapiens* genome, the hypothetical
739 intranuclear micro-pH [77] surrounding *H. sapiens* haploid interphase euchromatin when
740 covered (single quartet occupation) by the spermine tetracation alone can be calculated
741 $pH_{DNA/spermine}$ = 7.43. For the diploid dsDNA genome, after completed S phase during
742 interphase, the $pH_{DNA/spermine}$ is identical. The theoretical intranuclear micro-pH
743 surrounding *H. sapiens* haploid interphase euchromatin when covered (double triplet
744 occupation) by the sperminium phosphate/cyclooctaoxygen sodium complex can be
745 calculated $pH_{DNA/shell}$ = 7.42. For the diploid dsDNA genome, after completed S phase
746 during interphase, the $pH_{DNA/shell}$ is identical.

747 I also elaborated a model for selenium (as hydrogen selenite, $HSeO_3^-$, at
748 physiological pH 7.4) protection of DNA (Figure 12B) [5]. Selenium, the element of the
749 moon [78], was discovered by *Jöns Jacob Berzelius* (1779–1848) in 1817 and was
750 named by him in honor of the Greek goddess of the moon *Selene* (σελήνη) [79].

Preprints (www.preprints.org) | NOT PEER-REVIEWED | Posted: 4 December 2017 doi:10.20944/preprints201701.0086.v3

Selenium is essential to mammalian physiology at nutritional levels, but supraphysiological intake of selenium is known to be toxic for mammals [5,7]. Sodium selenite (Na_2SeO_3), as hydrogen selenite $HSeO_3^-$ at pH 7.0 (selenious acid H_2SeO_3: pK_{a1} = 2.62, pK_{a2} = 8.32 [80]), binds to calf thymus genomic B-DNA at pH 7.0 [81], and to *Saccharomyces cerevisiae* A-RNA at pH 7.0 [82]. Selenium has the ability to protect DNA from noxious influences (oxidative stress, radiation, cytotoxic agents) [5], and is essential to genomic stability [5,7,83,84], but the exact molecular biological basis for these phenomena is unknown. If in my model of a first epigenetic shell of *in vivo* DNA (Figure 12A) the monohydrogen phosphate is replaced by hydrogen selenite (Figure 12B), an epigenetic explanation for the interaction of selenium with eukaryotic *in vivo* DNA could be given. This model may account for, at least some of, the well-known bimodal, protective and toxic, *in vivo* effects exerted by selenium onto mammalian physiology [5,7]. A moderate substitution pattern of hydrogen selenite for monohydrogen phosphate would be essential, but if the displacement ratio $HSeO_3^-$ /HPO_4^{2-} exceeds a certain tolerance level, the epigenetic equilibrium should collapse. The extraordinary high, both acute and chronic, mammalian toxicity of sodium selenite (Na_2SeO_3) [85] should be due, at least in part, to direct detrimental effects of supraphysiological levels of hydrogen selenite $HSeO_3^-$ on mammalian chromosomal DNA integrity and regulation of genome expression. In fact, Na_2SeO_3 is a violent poison with a lethal dose 50% (LD_{50}, orally in rats, 7 mg/kg [86]), being lower than the LD_{50} of sodium cyanide (NaCN) (LD_{50}, orally in rats, 15 mg/kg [87]).

Assuming an essential biological function for the cyclooctaoxygen sodium-bridged spermine phosphate and selenite epigenetic shell, I searched for substances

Preprints (www.preprints.org) | NOT PEER-REVIEWED | Posted: 4 December 2017 doi:10.20944/preprints201701.0086.v3

able to *selectively* destroy this epigenetic protection structure, and tested the total herbicide glyphosate, *N*-(phosphonomethyl)glycine (ROUNDUP®, Monsanto), and its major environmental metabolite (aminomethyl)phosphonic acid (AMPA) [88] on the cyclo-O_8-Na^+ complex contained in **RC**. Glyphosate was chosen because it represents the top selling total herbicide worldwide [89], and **RC** was selected because of its highest molar cyclo-O_8-Na^+ content in the complex series **NC**, **dNC**, and **RC** (Figure 7) [5]. Glyphosate and AMPA show chemical properties which might predispose them for destruction of cyclooctaoxygen in general. Glyphosate and AMPA are very hydrophilic and amphoteric, and their phosphonate moieties could be suitable to interact with cyclo-O_8-Na^+. I could show unequivocally that glyphosate and AMPA indeed *selectively* destroy the cyclo-O_8-Na^+ complex contained in **RC** (Figure 3, 4, 10 and 11). I therefore conclude that glyphosate and the major environmental glyphosate metabolite AMPA [88] also destroy the cyclooctaoxygen sodium-bridged spermine phosphate and selenite epigenetic shell of human euchromatin, because destruction of cyclooctaoxygen is sufficient to bring this essential protection shield of human euchromatin into collateral epigenetic collapse.

To get support for the selectivity of AMPA as an epigenetic poison, the affinity of AMPA towards human mitochondrial γ-aminobutyric acid transaminase (ABAT) [33], and to wild-type human liver peroxisomal alanine:glyoxylate aminotransferase (AGT) [34], was determined. ABAT represents also a β-alanine transaminase [33], and both enzymes were selected because of the structural similarity between AMPA and β-alanine/L-alanine. AMPA showed essentially no affinity to ABAT, but was very slowly catabolized by AGT (Figure 5A). This latter result is of interest, since the product of the

Preprints (www.preprints.org) | NOT PEER-REVIEWED | Posted: 4 December 2017 doi:10.20944/preprints201701.0086.v3

half-transamination of AMPA by AGT is phosphonoformaldehyde which can be oxidized (peroxisomal glycolate oxidase, cytoplasmic lactate dehydrogenase [90]) to phosphonoformic acid (phosphonoformate, foscarnet) (Figure 5B). Foscarnet represents a well-known inhibitor of mammalian [91,92] and viral [91,92] DNA-dependent DNA polymerases. Eukaryotic DNA polymerase α is crucially involved in chromosome maintenance, DNA repair and recombination, transcriptional silencing, checkpoint activation, and telomere length maintenance [93]. Mammalian DNA polymerase α is potently inhibited by foscarnet [91,92]. Therefore, the low-affinity half-transamination of AMPA by AGT, the rate-limiting step leading to foscarnet, could negatively influence human chromosome maintenance, DNA damage repair, and telomere length preservation, mediated by the AMPA catabolite foscarnet inhibition of DNA polymerase α. This enzymatic catabolism provides an additional, minor mechanism of destabilization and impairment of eukaryotic chromosomal DNA indirectly induced by the environmental glyphosate metabolite AMPA.

Conclusion

I allow me the profound conclusion that the sperminium phosphate/cyclo-O_8-Na^+ coverage of nucleic acids is essential for eukaryotic gene regulation, and, in conjunction with selenite, protects and stabilizes gene-rich ‘open’ chromatin euchromatic DNA [5]. These postulations [5] would account for a long-sought molecular explanation of the essential, but ‘mysterious’ function of the polyamine spermine in eukaryotes [6]. Spermine is found only in eukaryotes, with some exceptions, and prokaryotes rely mostly on putrescine and spermidine [6,94]. The essentiality of spermine for humans is

Preprints (www.preprints.org) | NOT PEER-REVIEWED | Posted: 4 December 2017 doi:10.20944/preprints201701.0086.v3

820 exemplified by the *Snyder–Robinson* X-linked mental retardation syndrome [95] caused
821 by missense mutations in the human spermine synthase gene, leading to mental
822 retardation, generalised seizures, absent speech, inability to stand, and other severe
823 defects [95]. One can speculate that at the transition from prokaryotic to eukaryotic life
824 the sperminium phosphate/cyclo-O_8-Na^+ complex resulted as a consequence from the
825 combined accumulation of atmospheric oxygen and prokaryotic RNA, since the
826 evolution of spermine synthases from prokaryotic spermidine synthase was proposed
827 [94] as co-occurring with the onset of proto-eukaryotic life.

828 An improved and corrected molecular biological model is proposed for a first
829 epigenetic shell of eukaryotic euchromatin. This model incorporates an epigenetic
830 explanation for the interactions of the essential micronutrient selenium (as selenite) with
831 eukaryotic euchromatin. The sperminium phosphate/cyclooctaoxygen sodium complex
832 was calculated to cover the actively transcribed regions (2.6%) of bovine lymphocyte
833 interphase genome dsDNA (double occupation). The polyamine (spermine/spermidine
834 ratio 1.17) coverage of HeLa S3 cell metaphase chromatin dsDNA was calculated as
835 93.4% (single occupation). In murine cryptal enterocytic mitotic (late anaphase/early
836 telophase) chromatin the obtained *in vivo* value corresponds to complete genomic
837 coverage (single occupation), and to comprehensive and extensive nuclear RNA
838 coverage, by the spermine tetracation and spermidine trication (spermine/spermidine
839 ratio 0.85). Because cyclooctaoxygen seems to be naturally absent in hypoxia-induced
840 highly condensed chromatin [4], I hence propose a model [96] for the cyclooctaoxygen
841 sodium-bridged spermine phosphate (and selenite) epigenetic shell of actively
842 transcribed gene regions in eukaryotic ‘open’ chromatin DNA (Figure 13). Furthermore,

Preprints (www.preprints.org) | NOT PEER-REVIEWED | Posted: 4 December 2017 doi:10.20944/preprints201701.0086.v3

a working model is tabulated in summary for the selective cell cycle-dependent epigenetic occupation of eukaryotic DNA (Table 1).

What may be the overall biological significance, and pathophysiological implication, of this selective epigenetic shell? During transcription of actively transcribed gene regions in eukaryotic ‘open’ chromatin the double helix must be unwound by DNA helicases [97] and the strands must be separated to enable access to DNA-dependent RNA polymerases I, II [98,99], and III. This creates intermediate DNA single-strand regions which are prone to chemical structure damage by multiple noxious impacts like reactive oxygen species (ROS) [3] and mutagens [100]. The selective cyclooctaoxygen sodium-bridged spermine phosphate (and selenite) epigenetic occupation of these sensitive single-stranded stretches could serve as an intrinsic protection against chemically-induced structural damage. This would be a logic explanation for the selective nature of the separate occupation of both DNA strands, consequently retained when strands are separated for transcription of mRNA.

But what is the chemical, obviously evolutionary conserved, genomic necessity for the DNA single-strand protection by cyclooctaoxygen sodium-bridged spermine complexes? Since spontaneous deamination, ROS, chemical mutagens, and UV light do damage both dsDNA and ssDNA regions [101–103], albeit ssDNA with higher propensity than dsDNA [101,102], the immediate benefit must be based in another origin. Intriguing seem to be pH effects, since spermine is a strong base, and the major pH-related damage to DNA is depurination creating apurinic sites at low pH [104–106], with a four times higher reaction rate for ssDNA than for dsDNA [104,106].

Preprints (www.preprints.org) | NOT PEER-REVIEWED | Posted: 4 December 2017 doi:10.20944/preprints201701.0086.v3

865 The formation of kinetin (N^6-furfuryl-9*H*-adenine) from DNA is known [107]. It
866 should be emphasized that kinetin is not contained in native mammalian DNA, contrary
867 to misleading claims [108,109], but is formed only during DNA damage. A mechanism
868 for the kinetin formation in, or from, DNA was proposed [108,109], but it seems not to be
869 conclusive in chemical reason, since furfural does not react with the adenine 6-NH_2
870 group under condensation to a *Schiff* base [107]. I therefore propose a chemical
871 mechanistic deduced logical scheme [110–113] for the generation of kinetin from DNA
872 by proton catalysis (kinetin-generating “base flip”, KGBF) (Figure 14), based on proton-
873 catalysed depurination and subsequent inverted adenine 6-NH_2 *N*-glycosylation
874 [110,111], in consequence leaving back a DNA single-strand break. It is proposed that
875 the cyclooctaoxygen sodium-bridged spermine phosphate epigenetic shell protects
876 ssDNA from low pH-induced depurination, including, in part, generation of kinetin by
877 KGBF. This is substantiated by the precise calculation of the apparent acid dissociation
878 constant of the human genome DNA.

879 I therefore conclude that the sperminium phosphate/cyclooctaoxygen sodium
880 complex serves to protect ssDNA from nucleic acid-mediated intrinsic low intranuclear
881 micro-pH-induced depurination, including KGBF, creating apurinic sites and
882 concomitant DNA single-strand breaks at eukaryotic genome regions engaged in active
883 transcription. The precisely calculated intranuclear micro-pH gain, obtained by
884 sperminium phosphate/cyclooctaoxygen sodium complexation of B-DNA individual
885 strands, is essentially the same as the intranuclear micro-pH gain for condensed B-DNA
886 strand-overarchingly covered by sperminium tetracations.

Preprints (www.preprints.org) | NOT PEER-REVIEWED | Posted: 4 December 2017 doi:10.20944/preprints201701.0086.v3

In conclusion, it is logically obvious that any chemical agent, biochemical precursor (selenium) deficiency, and/or physical circumstance compromising the sperminium phosphate/selenite–cyclooctaoxygen sodium complexation will inevitably lead to a severe disturbation of eukaryotic genome integrity, to an increased mutation rate, and to genomic DNA single-strand breaks caused by KGBF. This is, in part, proved by the *Snyder–Robinson* X-linked mental retardation syndrome [95], characterized by a defect in spermine synthesis, leading to nearly complete loss of the polyamine spermine. I therefore investigated chemical agents selectively destroying the epigenetic shell of eukaryotic euchromatin, found a candidate molecule, and, hence, wish to define it as an 'epigenetic poison'. The total herbicide glyphosate, *N*-(phosphonomethyl)glycine (ROUNDUP®, Monsanto), and its major environmental metabolite (aminomethyl)phosphonic acid (AMPA) [88] were found, rather unequivocally, to selectively destroy the cyclo-O_8-Na^+ complex contained in **RC** (Figure 3, 4, 10 and 11). Glyphosate and AMPA came into focus because (i) glyphosate represents the top selling total herbicide worldwide [89], (ii) their chemical structure (phosphonate + amine) and properties (strongly hydrophilic and acidic) seemed to enable them to interact with cyclooctaoxygen sodium, (iii) glyphosate and ROUNDUP® are suspected to damage DNA and cause cancer in humans [114], and (iv) AMPA is already widely distributed in global ecosystems like (surface) water [115].

I allow me to conclude on basis of my, rather unequivocal, findings that glyphosate, ROUNDUP® and AMPA are major examples of slow-acting, insidious 'epigenetic poisons', (i) slowly eroding and detoriating human, animal and plant genomic integrity, (ii) rattening human, animal and plant inborne protection of hereditary

information against mutation, and (iii) disturbing the processing of human, animal and plant genetic information by transcription. It is hence inevitable for me to define glyphosate, ROUNDUP® and AMPA as a significant threat for human, animal and plant genomic stability, especially for future human generations forced to live under the glyphosate-, ROUNDUP®- and AMPA-induced radiomimetic effects. The evidence presented here also indirectly shows that glyphosate, ROUNDUP® and AMPA must acting carcinogenic [116] and teratogenic [117] in humans with respect to their detrimental impact on human DNA structure. This was already proved to be the common outcome for some epigenetic poisons in the pesticide/herbicide field [116,117].

Acknowledgment

The author thanks T. Westfeld, E.-M. May, D. Wiegel, W. Wübbolt, O. Meier, R. Sachs, A. Karbach, W. Bergmeier, J. Moldenhauer and H.-J. Hühn (Currenta GmbH & Co. OHG, Leverkusen, Germany) for analytical services. I thank especially H.J. Jodl for helpful discussions, E.A. Struys (University Hospital Vrije Universiteit, Amsterdam, The Netherlands) for performing the ABAT assays, and B. Cellini (University of Perugia, Department of Experimental Medicine, Italy) for performing the AGT assays. The author is obliged to K. Hecker, K. Meuser and K. Hecker (HEKAtech GmbH, Wegberg, Germany) for expert elemental analyses.

Conflict of interest

The author declares no conflict of interest in this paper.

 doi:10.20944/preprints201701.0086.v3

References

1. van Leeuwenhoek A (1677–1678) Observationes D. Anthonii Lewenhoeck, de natis è semine genitali animalculis. Philos Trans R Soc Lond 12: 1040–1046.

2. Rosenheim O (1924) The isolation of spermine phosphate from semen and testis. Biochem J 18: 1253–1262.

3. Cooke MS, Evans MD, Dizdaroglu M, Lunec J (2003) Oxidative DNA damage: mechanisms, mutation, and disease. FASEB J 17: 1195–1214.

4. Kirmes I, Szczurek A, Prakash K, Charapitsa I, Heiser C, Musheev M, Schock F, Fornalczyk K, Ma D, Birk U, Cremer C, Reid G (2015) A transient ischemic environment induces reversible compaction of chromatin. Genome Biol 16: 246. doi:10.1186/s13059-015-0802-2.

5. Kesel AJ, Day CW, Montero CM, Schinazi RF (2016) A new oxygen modification cyclooctaoxygen binds to nucleic acids as sodium crown complex. Biochim Biophys Acta 1860: 785–794.

6. Igarashi K, Kashiwagi K (2000) Polyamines: mysterious modulators of cellular functions. Biochem Biophys Res Commun 271: 559–564.

7. Ferguson LR, Karunasinghe N, Zhu S, Wang AH (2012) Selenium and its' role in the maintenance of genomic stability. Mutat Res 733: 100–110.

8. Kuse R, Schuster S, Schübbe H, Dix S, Hausmann K (1985) Blood lymphocyte volumes and diameters in patients with chronic lymphocytic leukemia and normal controls. Blut (Berl) 50: 243–248.

954 9. Sipe CR, Chanana AD, Cronkite EP, Gulliani GL, Joel DD (1976) Studies on
955 lymphocytes XIII. Nuclear volume measurement as a rapid approach to estimate
956 proliferative fraction. Scand J Haematol 16: 196–201.

957 10. National Center for Biotechnology Information (NCBI) (2016)
958 Bos_taurus_UMD_3.1.1, Bethesda, MD, USA:
959 https://www.ncbi.nlm.nih.gov/assembly/GCF_000003055.6/.

960 11. Watanabe S, Kusama-Eguchi K, Kobayashi H, Igarashi K (1991) Estimation of
961 polyamine binding to macromolecules and ATP in bovine lymphocytes and rat
962 liver. J Biol Chem 266: 20803–20809.

963 12. National Center for Biotechnology Information (NCBI) (2016) GRCh38.p9,
964 Bethesda, MD, USA: https://www.ncbi.nlm.nih.gov/assembly/GCF_000001405.35/.

965 13. Adey A, Burton JN, Kitzman JO, Hiatt JB, Lewis AP, Martin BK, Qiu R, Lee C,
966 Shendure J (2013) The haplotype-resolved genome and epigenome of the
967 aneuploid HeLa cancer cell line. Nature 500: 207–211.

968 14. Macville M, Schröck E, Padilla-Nash H, Keck C, Ghadimi BM, Zimonjic D, Popescu
969 N, Ried T (1999) Comprehensive and definitive molecular cytogenetic
970 characterization of HeLa cells by spectral karyotyping. Cancer Res 59: 141–150.

971 15. Goyns MH (1979) Polyamine content of a non-aqueously isolated chromosome
972 preparation. Exp Cell Res 122: 377–380.

973 16. Jain S, Zon G, Sundaralingam M (1989) Base only binding of spermine in the deep
974 groove of the A-DNA octamer d(GTGTACAC). Biochemistry 28: 2360–2364.

17. Egli M, Williams LD, Gao Q, Rich A (1991) Structure of the pure-spermine form of Z-DNA (magnesium free) at 1-Å resolution. Biochemistry 30: 11388–11402.

18. Ohishi H, Nakanishi I, Inubushi K, van der Marel G, van Boom JH, Rich A, Wang AHJ, Hakoshima T, Tomita K (1996) Interaction between the left-handed Z-DNA and polyamine-2. The crystal structure of the $d(CG)_3$ and spermidine complex. FEBS Lett 391: 153–156.

19. Ohishi H, Tozuka Y, Da-Yang Z, Ishida T, Nakatani K (2007) The rare crystallographic structure of $d(CGCGCG)_2$: the natural spermidine molecule bound to the minor groove of left-handed Z-DNA $d(CGCGCG)_2$ at 10 °C. Biochem Biophys Res Commun 358: 24–28.

20. Cameron IL, Smith NKR, Pool TB (1979) Element concentration changes in mitotically active and postmitotic enterocytes. An X-ray microanalysis study. J Cell Biol 80: 444–450.

21. National Center for Biotechnology Information (NCBI) (2016) C3H_HeJ_v1, Bethesda, MD, USA: https://www.ncbi.nlm.nih.gov/assembly/738461.

22. Sarhan S, Seiler N (1989) On the subcellular localization of the polyamines. Biol Chem Hoppe-Seyler 370: 1279–1284.

23. Viola-Magni MP, Gahan PB, Pacy J (1985) Phospholipids in plant and animal chromatin. Cell Biochem Funct 3: 71–78.

24. Kumler WD, Eiler JJ (1943) The acid strength of mono and diesters of phosphoric acid. The n-alkyl esters from methyl to butyl, the esters of biological importance, and the natural guanidine phosphoric acids. J Am Chem Soc 65: 2355–2361.

 doi:10.20944/preprints201701.0086.v3

997 25. Katchalsky A, Gillis J (1949) Theory of the potentiometric titration of polymeric
998 acids. Recl Trav Chim Pays-Bas 68: 879–897.

999 26. Kuhn W, Kuhn H (1943) Die Frage nach der Aufrollung von Fadenmolekülen in
1000 strömenden Lösungen. Helv Chim Acta 26: 1394–1465.

1001 27. Mandelkern M, Elias JG, Eden D, Crothers DM (1981) The dimensions of DNA in
1002 solution. J Mol Biol 152: 153–161.

1003 28. Langridge R, Marvin DA, Seeds WE, Wilson HR, Hooper CW, Wilkins MHF,
1004 Hamilton LD (1960) The molecular configuration of deoxyribonucleic acid. II.
1005 Molecular models and their Fourier transforms. J Mol Biol 2: 38–64.

1006 29. Mermer A, Starynowicz P (2012) Charge-density distribution in potassium
1007 dihydrogen phosphoglycolate – a comparison of phosphate and phosphonate
1008 groups. Acta Crystallogr B 68: 625–635.

1009 30. Aikens D, Bunce S, Onasch F, Parker R, III., Hurwitz C, Clemans S (1983) The
1010 interactions between nucleic acids and polyamines. II. Protonation constants and
1011 ^{13}C-NMR chemical shift assignments of spermidine, spermine, and homologs.
1012 Biophys Chem 17: 67–74.

1013 31. Tari LW, Secco AS (1995) Base-pair opening and spermine binding—B-DNA
1014 features displayed in the crystal structure of a *gal* operon fragment: implications for
1015 protein–DNA recognition. Nucleic Acids Res 23: 2065–2073.

1016 32. Wiberg, N. (Editor) (1995) Holleman–Wiberg, Lehrbuch der Anorganischen
1017 Chemie (101st Edition), Berlin/New York: Walter de Gruyter, 771.

 doi:10.20944/preprints201701.0086.v3

1018 33. Shor DSM, Struys EA, Hogema BM, Gibson KM, Jakobs C (2001) Development of
1019 a stable-isotope dilution assay for γ-aminobutyric acid (GABA) transaminase in
1020 isolated leukocytes and evidence that GABA and β-alanine transaminases are
1021 identical. Clin Chem 47: 525–531.

1022 34. Cellini B, Montioli R, Bianconi S, López-Alonso JP, Borri Voltattorni C (2008)
1023 Construction, purification and characterization of untagged human liver alanine-
1024 glyoxylate aminotransferase expressed in *Escherichia coli*. Protein Pept Lett 15:
1025 153–159.

1026 35. Oppici E, Fodor K, Paiardini A, Williams C, Borri Voltattorni C, Wilmanns M, Cellini,
1027 B (2013) Crystal structure of the S187F variant of human liver alanine: glyoxylate
1028 aminotransferase associated with primary hyperoxaluria type I and its functional
1029 implications. Proteins 81: 1457–1465; Erratum published (2013): Proteins 82: 171.

1030 36. Freiman YuA, Jodl HJ (2004) Solid oxygen. Phys Rep 401: 1–288.

1031 37. Lundegaard LF, Weck G, McMahon MI, Desgreniers S, Loubeyre P (2006)
1032 Observation of an O_8 molecular lattice in the ε phase of solid oxygen. Nature 443:
1033 201–204.

1034 38. Kim KS, Jang JH, Kim S, Mhin B-J, Schaefer HF, III. (1990) Potential new high
1035 energy density materials: cyclooctaoxygen O_8, including comparisons with the
1036 well-known cyclo-S_8 molecule. J Chem Phys 92: 1887–1892.

1037 39. Shapiro R, Agarwal SC (1968) Reaction of ninhydrin with cytosine derivatives. J
1038 Am Chem Soc 90: 474–478.

 doi:10.20944/preprints201701.0086.v3

1039 40. Doherty EA, Doudna JA (2001) Ribozyme structures and mechanisms. Annu Rev
1040 Biophys Biomol Struct 30: 457–475.

1041 41. Mielcarek M, Barciszewska MZ, Sałanski P, Stobiecki M, Jurczak J, Barciszewski
1042 J (2002) Native transfer RNA catalyzes Diels–Alder reaction. Biochem Biophys
1043 Res Commun 294: 145–148.

1044 42. Ruzin A, Severin A, Ritacco F, Tabei K, Singh G, Bradford PA, Siegel MM, Projan
1045 SJ, Shlaes DM (2002) Further evidence that a cell wall precursor [C_{55}-MurNAc-
1046 (peptide)-GlcNAc] serves as an acceptor in a sorting reaction. J Bacteriol 184:
1047 2141–2147.

1048 43. Watson JD, Crick FHC (1953) Genetical implications of the structure of
1049 deoxyribonucleic acid. Nature 171: 964–967.

1050 44. Herbstein FH, Kapon M, Schwotzer W (1983) Crystal structure of
1051 tetrakis(phenacetin) dihydrogentetraiodide dihydrate {[$H_5C_2OC_6H_4N(H)C(CH_3)=O]_4$
1052 • H_2I_4 • 2 H_2O}. Helv Chim Acta 66: 35–43.

1053 45. Hitchcock PB, Hughes DL, Leigh GJ, Sanders JR, de Souza J, McGarry CJ,
1054 Larkworthy LF (1994) Preparation of new vanadium(II) iodides and crystal
1055 structure of hexakis(acetonitrile)vanadium(II) (tetraiodide). J Chem Soc, Dalton
1056 Trans: 3683–3687.

1057 46. Genser EE, Connick RE (1973) Exchange of iodide ion with triiodide ion studied by
1058 nuclear magnetic resonance. J Chem Phys 58: 990–996.

1059 47. Schenck H-U, Simak P, Haedicke E (1979) Structure of polyvinylpyrrolidone-iodine
1060 (povidone-iodine). J Pharm Sci 68: 1505–1509.

1061 48. Herbstein FH, Kapon M (1972) Zigzag chains of alternating iodine molecules and
1062 triiodide ions in crystalline $(phenacetin)_2 \cdot HI_5$. Nature Phys Sci 239: 153–154.

1063 49. Saenger W (1984) The structure of the blue starch–iodine complex.
1064 Naturwissenschaften 71: 31–36.

1065 50. Svensson PH, Kloo L (2003) Synthesis, structure, and bonding in polyiodide and
1066 metal iodide–iodine systems. Chem Rev 103: 1649–1684.

1067 51. Tomlin CDS (Editor) (1997) The pesticide manual: a world compendium,
1068 incorporating the agrochemicals handbook (11^{th} Edition), Farnham/Surrey (UK):
1069 British Crop Protection Council.

1070 52. Terpstra KR, Woortman AJJ, Hopman JCP (2010) Yellow dextrins: evaluating
1071 changes in structure and colour during processing. Starch/Stärke 62: 449–457.

1072 53. Cellini B, Bertoldi M, Montioli R, Paiardini A, Borri Voltattorni C (2007) Human wild-
1073 type alanine:glyoxylate aminotransferase and its naturally occurring G82E variant:
1074 functional properties and physiological implications. Biochem J 408: 39–50.

1075 54. Schuster H, Schramm G, Zillig W (1956) Die Struktur der Ribonucleinsäure aus
1076 Tabakmosaikvirus. Z Naturforsch B 11: 339–345.

1077 55. Lever MA, Torti A, Eickenbusch P, Michaud AB, Šantl-Temkiv T, Jørgensen BB
1078 (2015) A modular method for the extraction of DNA and RNA, and the separation
1079 of DNA pools from diverse environmental sample types. Front Microbiol 6: 476.
1080 doi:10.3389/fmicb.2015.00476.

1081 56. Binns EH (1959) The dissociation constant of phenol in water between 25°C and
1082 60°C. Trans Faraday Soc 55: 1900–1903.

 doi:10.20944/preprints201701.0086.v3

1083 57. Takeda Y, Samejima K, Nagano K, Watanabe M, Sugeta H, Kyogoku Y (1983)
1084 Determination of protonation sites in thermospermine and in some other
1085 polyamines by ^{15}N and ^{13}C nuclear magnetic resonance spectroscopy. Eur J
1086 Biochem 130: 383–389.

1087 58. Fukuzumi S, Yorisue T (1991) Quinone/hydroxide ion induced oxygenation of p-
1088 benzoquinone to rhodizonate dianion ($C_6O_6^{2-}$) accompanied by one-electron
1089 reduction to semiquinone radical anion. J Am Chem Soc 113: 7764–7765.

1090 59. Vogel F, Harf J, Hug A, von Rohr PR (1999) Promoted oxidation of phenol in
1091 aqueous solution using molecular oxygen at mild conditions. Environ Prog 18:
1092 7–13.

1093 60. Kay ERM, Simmons NS, Dounce AL (1952) An improved preparation of sodium
1094 desoxyribonucleate. J Am Chem Soc 74: 1724–1726.

1095 61. Emanuel CF, Chaikoff IL (1953) The large scale preparation of sodium
1096 desoxyribonucleate from ripe salmon testes. J Biol Chem 203: 167–171.

1097 62. Waddington CH (1942) The epigenotype. Endeavour (Engl Ed Lond) 1: 18–20.

1098 63. Crick FHC, Watson JD (1954) The complementary structure of deoxyribonucleic
1099 acid. Proc R Soc Lond A Math Phys Sci 223: 80–96.

1100 64. Schlegel MK, Essen L-O, Meggers E (2008) Duplex structure of a minimal nucleic
1101 acid. J Am Chem Soc 130: 8158–8159.

1102 65. Heinemann U, Lauble H, Frank R, Blöcker H (1987) Crystal structure analysis of
1103 an A-DNA fragment at 1.8 Å resolution: d(GCCCGGGC). Nucleic Acids Res 15:
1104 9531–9550.

66. Mandal PK, Venkadesh S, Gautham N (2012) Structure of the tetradecanucleotide d(CCCCGGTACCGGGG)$_2$ as an A-DNA duplex. Acta Crystallogr Sect F Struct Biol Cryst Commun 68: 393–399.

67. Saenger W, Hunter WN, Kennard O (1986) DNA conformation is determined by economics in the hydration of phosphate groups. Nature 324: 385–388.

68. Leder P, Nirenberg M (1964) RNA codewords and protein synthesis, II. Nucleotide sequence of a valine RNA codeword. Proc Natl Acad Sci USA 52: 420–427.

69. Sunkara PS, Ramakrishna S, Nishioka K, Rao PN (1981) The relationship between levels and rates of synthesis of polyamines during mammalian cell cycle. Life Sci 28: 1497–1506.

70. Li G, Sudlow G, Belmont AS (1998) Interphase cell cycle dynamics of a late-replicating, heterochromatic homogeneously staining region: precise choreography of condensation/decondensation and nuclear positioning. J Cell Biol 140: 975–989.

71. Matera AG, Terns RM, Terns MP (2007) Non-coding RNAs: lessons from the small nuclear and small nucleolar RNAs. Nat Rev Mol Cell Biol 8: 209–220.

72. Llères D, James J, Swift S, Norman DG, Lamond AI (2009) Quantitative analysis of chromatin compaction in living cells using FLIM–FRET. J Cell Biol 187: 481–496.

73. Thomas TJ, Gunnia UB, Thomas T (1991) Polyamine-induced B-DNA to Z-DNA conformational transition of a plasmid DNA with (dG-dC)$_n$ insert. J Biol Chem 266: 6137–6141.

74. Deng H, Bloomfield VA, Benevides JM, Thomas GJ, Jr. (2000) Structural basis of polyamine–DNA recognition: spermidine and spermine interactions with genomic B-DNAs of different GC content probed by Raman spectroscopy. Nucleic Acids Res 28: 3379–3385.

75. Rich A, Zhang S (2003) Z-DNA: the long road to biological function. Nat Rev Genet 4: 566–572.

76. Ha SC, Lowenhaupt K, Rich A, Kim Y-G, Kim KK (2005) Crystal structure of a junction between B-DNA and Z-DNA reveals two extruded bases. Nature 437: 1183–1186.

77. Rhodes CT (1999) Determination of micro-pH in solid drug delivery systems. Drug Dev Ind Pharm 25: 1221–1222.

78. Flohé L, Andreesen JR, Brigelius-Flohé R, Maiorino M, Ursini F (2000) Selenium, the element of the moon, in life on earth. IUBMB Life 49: 411–420.

79. Berzelius JJ (1817) Lettre de M. Berzelius à M. Berthollet sur deux Métaux nouveaux. Ann Chim Phys (Paris) 7: 199–206.

80. Borah S, Kumar PP (2016) *Ab initio* molecular dynamics study of Se(IV) species in aqueous environment. Phys Chem Chem Phys 18: 26755–26763.

81. Nafisi S, Montazeri M, Manouchehri F (2012) The effect of Se salts on DNA structure. J Photochem Photobiol B 113: 36–41.

82. Nafisi S, Manouchehri F, Montazeri M (2011) RNA adducts with Na_2SeO_4 and Na_2SeO_3 – Stability and structural features. J Mol Struct 1006: 547–552.

 doi:10.20944/preprints201701.0086.v3

1148 83. Wu J, Lyons GH, Graham RD, Fenech MF (2009) The effect of selenium, as
1149 selenomethionine, on genome stability and cytotoxicity in human lymphocytes
1150 measured using the cytokinesis-block micronucleus cytome assay. Mutagenesis
1151 24: 225–232.

1152 84. Graupner A, Instanes C, Andersen JM, Brandt-Kjelsen A, Dertinger SD, Salbu B,
1153 Brunborg G, Olsen A-K (2015) Genotoxic effects of two-generational selenium
1154 deficiency in mouse somatic and testicular cells. Mutagenesis 30: 217–225.

1155 85. Abdo KM (1994) National Toxicology Program (NTP). Technical report on toxicity
1156 studies of sodium selenate and sodium selenite (CAS Nos. 13410-01-0 and
1157 10102-18-8) administered in drinking water to F344/N rats and B6C3F$_1$ mice (NIH
1158 Publication 94-3387). Toxic Rep Ser 38: 1–127.

1159 86. Cummins LM, Kimura ET (1971) Safety evaluation of selenium sulfide antidandruff
1160 shampoos. Toxicol Appl Pharmacol 20: 89–96.

1161 87. Smyth HF, Jr., Carpenter CP, Weil CS, Pozzani UC, Striegel JA, Nycum JS (1969)
1162 Range-finding toxicity data: List VII. Am Ind Hyg Assoc J 30: 470–476.

1163 88. Rueppel ML, Brightwell BB, Schaefer J, Marvel JT (1977) Metabolism and
1164 degradation of glyphosate in soil and water. J Agric Food Chem 25: 517–528.

1165 89. Benbrook CM (2016) Trends in glyphosate herbicide use in the United States and
1166 globally. Environ Sci Eur 28: 3. doi:10.1186/s12302-016-0070-0.

1167 90. Holmes RP, Assimos DG (1998) Glyoxylate synthesis, and its modulation and
1168 influence on oxalate synthesis. J Urol 160: 1617–1624.

1169 91. Helgstrand E, Eriksson B, Johansson NG, Lannerö B, Larsson A, Misiorny A,
1170 Norén JO, Sjöberg B, Stenberg K, Stening G, Stridh S, Öberg B, Alenius S,
1171 Philipson L (1978) Trisodium phosphonoformate, a new antiviral compound.
1172 Science 201: 819–821.

1173 92. Sabourin CLK, Reno JM, Boezi JA (1978) Inhibition of eucaryotic DNA
1174 polymerases by phosphonoacetate and phosphonoformate. Arch Biochem
1175 Biophys 187: 96–101.

1176 93. Khan S, Ahmed S (2015) Role of *swi7H4* mutant allele of DNA polymerase α in
1177 the DNA damage checkpoint response. PLoS One 10: e0124063.
1178 doi:10.1371/journal.pone.0124063.

1179 94. Minguet EG, Vera-Sirera F, Marina A, Carbonell J, Blázquez MA (2008)
1180 Evolutionary diversification in polyamine biosynthesis. Mol Biol Evol 25:
1181 2119–2128.

1182 95. de Alencastro G, McCloskey DE, Kliemann SE, Maranduba CMC, Pegg AE, Wang
1183 X, Bertola DR, Schwartz CE, Passos-Bueno MR, Sertié AL (2008) New *SMS*
1184 mutation leads to a striking reduction in spermine synthase protein function and a
1185 severe form of Snyder–Robinson X-linked recessive mental retardation syndrome.
1186 J Med Genet 45: 539–543.

1187 96. Rosa S, Shaw P (2013) Insights into chromatin structure and dynamics in plants.
1188 Biology 2: 1378–1410. doi:10.3390/biology2041378.

1189 97. van Brabant AJ, Stan R, Ellis NA (2000) DNA helicases, genomic instability, and
1190 human genetic disease. Annu Rev Genomics Hum Genet 1: 409–459.

1191 98. Cramer P, Bushnell DA, Kornberg RD (2001) Structural basis of transcription: RNA
1192 polymerase II at 2.8 Ångstrom resolution. Science 292: 1863–1876.

1193 99. Bernecky C, Herzog F, Baumeister W, Plitzko JM, Cramer P (2016) Structure of
1194 transcribing mammalian RNA polymerase II. Nature 529: 551–554.

1195 100. Ames BN (1979) Identifying environmental chemicals causing mutations and
1196 cancer. Science 204: 587–593.

1197 101. Chan K, Sterling JF, Roberts SA, Bhagwat AS, Resnick MA, Gordenin DA (2012)
1198 Base damage within single-strand DNA underlies *in vivo* hypermutability induced
1199 by a ubiquitous environmental agent. PLoS Genet 8: e1003149.
1200 doi:10.1371/journal.pgen.1003149.

1201 102. Vodička P, Hemminki K (1988) Identification of alkylation products of styrene oxide
1202 in single- and double-stranded DNA. Carcinogenesis 9: 1657–1660.

1203 103. Gordon LK, Haseltine WA (1982) Quantitation of cyclobutane pyrimidine dimer
1204 formation in double- and single-stranded DNA fragments of defined sequence.
1205 Radiat Res 89: 99–112.

1206 104. Lindahl T (1993) Instability and decay of the primary structure of DNA. Nature 362:
1207 709–715.

1208 105. Lindahl T, Nyberg B (1972) Rate of depurination of native deoxyribonucleic acid.
1209 Biochemistry 11: 3610–3618.

1210 106. Loeb LA, Preston BD (1986) Mutagenesis by apurinic/apyrimidinic sites. Ann Rev
1211 Genet 20: 201–230.

 doi:10.20944/preprints201701.0086.v3

1212 107. Miller CO, Skoog F, Okumura FS, von Saltza MH, Strong FM (1956) Isolation,
1213 structure and synthesis of kinetin, a substance promoting cell division. J Am Chem
1214 Soc 78: 1375–1380.

1215 108. Barciszewski J, Siboska GE, Pedersen BO, Clark BFC, Rattan SIS (1997) A
1216 mechanism for the in vivo formation of N^6-furfuryladenine, kinetin, as a secondary
1217 oxidative damage product of DNA. FEBS Lett 414: 457–460.

1218 109. Barciszewski J, Massino F, Clark BFC (2007) Kinetin—a multiactive molecule. Int
1219 J Biol Macromol 40: 182–192.

1220 110. Fuller WD, Sanchez RA, Orgel LE (1972) Studies in prebiotic synthesis. VI.
1221 Synthesis of purine nucleosides. J Mol Biol 67: 25–33.

1222 111. Maurel M-C, Convert O (1990) Chemical structure of a prebiotic analog of
1223 adenosine. Orig Life Evol Biosph 20: 43–48.

1224 112. Mustard TJL, Mack DJ, Njardarson JT, Cheong PH-Y (2013) Mechanism and the
1225 origins of stereospecificity in copper-catalyzed ring expansion of vinyl oxiranes: a
1226 traceless dual transition-metal-mediated process. J Am Chem Soc 135:
1227 1471–1475.

1228 113. Ilardi EA, Njardarson JT (2013) Ring expansions of vinyloxiranes, -thiiranes, and -
1229 aziridines: synthetic approaches, challenges, and catalytic success stories. J Org
1230 Chem 78: 9533–9540.

1231 114. Koller VJ, Fürhacker V, Nersesyan A, Mišík M, Eisenbauer M, Knasmueller S
1232 (2012) Cytotoxic and DNA-damaging properties of glyphosate and Roundup in
1233 human-derived buccal epithelial cells. Arch Toxicol 86: 805–813.

 doi:10.20944/preprints201701.0086.v3

1234 115. Coupe RH, Kalkhoff SJ, Capel PD, Gregoire C (2012) Fate and transport of
1235 glyphosate and aminomethylphosphonic acid in surface waters of agricultural
1236 basins. Pest Manag Sci 68: 16–30. doi:10.1002/ps.2212.

1237 116. Rakitsky VN, Koblyakov VA, Turusov VS (2000) Nongenotoxic (epigenetic)
1238 carcinogens: pesticides as an example. A critical review. Teratog Carcinog
1239 Mutagen 20: 229–40.

1240 117. Bishop JB, Witt KL, Sloane RA (1997) Genetic toxicities of human teratogens.
1241 Mutat Res 396: 9–43.

Preprints (www.preprints.org) | NOT PEER-REVIEWED | Posted: 4 December 2017 doi:10.20944/preprints201701.0086.v3

Cell cycle phase		Heterochromatin		Euchromatin	
Interphase	**Function (concise)**	**Spermine-occupation?**	**Cyclo-O_8-Na^+-occupation?**	**Spermine-occupation?**	**Cyclo-O_8-Na^+-occupation?**
G_0 (Gap 0)	Resting and quiescence	No	No	Yes (2 ×) – With cyclo-O_8-Na^+	Yes (2 ×) – On 'open' Chr
G_1 (Gap 1)	Transcription and histone synthesis	No	No	Yes (2 ×) – With cyclo-O_8-Na^+	Yes (2 ×) – On 'open' Chr
S (Synthesis)	DNA synthesis	No	No	Yes (2 ×) – With cyclo-O_8-Na^+	Yes (2 ×) – On 'open' Chr
G_2 (Gap 2)	Translation	No	No	Yes (2 ×) – With cyclo-O_8-Na^+	Yes (2 ×) – On 'open' Chr
Mitosis	**Function (concise)**	**Spermine-occupation?**	**Cyclo-O_8-Na^+-occupation?**	**Spermine-occupation?**	**Cyclo-O_8-Na^+-occupation?**
Prophase	Chr condenses into chromosomes, nucleolus disappears	Yes (1 ×) – Condensing Chr	No	Yes (1 ×) – Condensing Chr	No
Prometaphase	Kinetochore and polar microtubules attach, mitotic spindle formed, nucleus disappears	Yes (1 ×) – Condensed Chr	No	Yes (1 ×) – Condensed Chr	No
Metaphase	Centrosomes pull chromosomes, chromosome centromeres line up at metaphase plate	Yes (1 ×) – Highly condensed Chr	No	Yes (1 ×) – Highly condensed Chr	No
Anaphase	Chromosomes break at centromeres, sister chromatids separated by microtubules	Yes (1 ×) – Maximally condensed Chr in late anaphase	No	Yes (1 ×) – Maximally condensed Chr in late anaphase	No
Telophase	Chr reformed from chromosomes, nucleus and nucleolus reappear	Yes (1 ×) – Maximally condensed Chr in early telophase	No	Yes (1 ×) – Maximally condensed Chr in early telophase	No

1242 **Table 1:** Tabulation of the selective cell cycle-dependent occupation of eukaryotic DNA
1243 by epigenetic polyamine shells. 1 ×, single quartet occupation (one polyamine *pro* both
1244 strands); 2 ×, double triplet occupation (one polyamine *pro* one strand); Chr, chromatin.

Preprints (www.preprints.org) | NOT PEER-REVIEWED | Posted: 4 December 2017 doi:10.20944/preprints201701.0086.v3

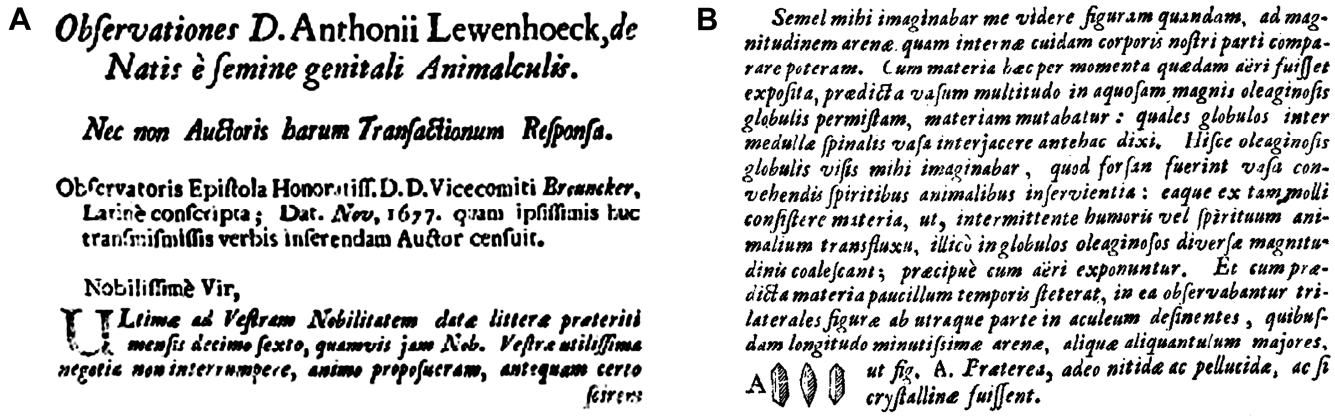

A

Observationes D. Anthonii Lewenhoeck, de Natis è semine genitali Animalculis.

Nec non Auctoris harum Transactionum Responsa.

Observatoris Epistola Honoratiss. D. D. Vicecomiti *Brouncker*, Latinè conscripta; Dat. *Nov*, 1677. quam ipsissimis huc transmissis verbis inserendam Auctor censuit.

Nobilissimè Vir,

Ultimæ ad Vestram Nobilitatem datæ litteræ præteriti mensis decimo sexto, quamvis jam Nob. Vestræ utilissima negotia non interrumpere, animo proposueram, antequam certo scirem

B

Semel mihi imaginabar me videre figuram quandam, ad magnitudinem arenæ, quam internæ cuidam corporis nostri parti comparare poteram. Cum materia hæc per momenta quædam aëri fuisset exposita, prædicta vasum multitudo in aquosam magnis oleaginosis globulis permistam, materiam mutabatur: quales globulos inter medullæ spinalis vasa interjacere antehac dixi. Hisce oleaginosis globulis visis mihi imaginabar, quod forsan fuerint vasa convehendis spiritibus animalibus inservientia: eaque ex tam molli consistere materia, ut, intermittente humoris vel spirituum animalium transfluxu, illicò in globulos oleaginosos diversæ magnitudinis coalescant; præcipuè cum aëri exponuntur. Et cum prædicta materia paucillum temporis steterat, in ea observabantur trilaterales figuræ ab utraque parte in aculeum desinentes, quibusdam longitudo minutissimæ arenæ, aliquæ aliquantulum majores, A *ut fig.* A. *Prætera, adeo nitidæ ac pellucidæ, ac si crystallinæ fuissent.*

Figure 1: Parts of the original publication [1] from 1677 by *Antoni van Leeuwenhoek* with the description of the first light microscopic observation of crystalline spermine phosphate in human semen, (A) the title page 1040, (B) page 1042 with fig. A showing the characteristic crystalline shape [2] of spermine × 2 H_3PO_4 × 6 H_2O [2]. The last paragraph including fig. A is read in New Latin: "*Et sum prædicta materia paucillum temporis steterat, in ea observabantur trilaterales figuræ ab utraque parte in aculeum desinentes, quibusdam longitudo minutissimæ arenæ, aliquæ aliquantulum majores, ut fig. A. Prætera, adeo nitidæ ac pellucidæ, ac si crystallinæ fuissent.*". English transcription: "*And I mentioned the matter which stood for a short time, in which trilateral figures were observed from both sides ending in a sting, some in length of minute grains, some a little larger, as fig. A. Moreover, so sleek and translucent, as if it were crystalline.*".

Preprints (www.preprints.org) | NOT PEER-REVIEWED | Posted: 4 December 2017 doi:10.20944/preprints201701.0086.v3

A

$$pK'_{a,HG} = \frac{8}{3}(n-1) + pK_{a,R-OH} = 7.1849$$

$$\text{with } (n-1) = \frac{0.821 \times 10^{-5}\ \text{cm} \times \lambda}{\sqrt[3]{2\,\lambda' sjb^2}}, \text{ and } \lambda = 1 + \ln\frac{3\,h_v^2}{2\,h_0^2};\ \lambda' = \ln\frac{3\,h_v^2}{2\,h_0^2} - 1$$

B

$$pH_{DNA} = -\log_{10}\sqrt{10^{-pK'_{a,HG}} \times c_{DNA} \times 3{,}238{,}442{,}024 \times 2 \times 2.6862\%} = 1.6642$$

$$pH_{spermine} = -\log_{10}\sqrt{\frac{10^{-14} \times 10^{-pK'_{spermine}}}{c_{DNA} \times \frac{1}{4} \times 3{,}238{,}442{,}024 \times 2.6862\%}} = 13.1867$$

$$pH_{shell} = -\log_{10}\sqrt{\frac{10^{-14} \times 10^{-pK'_{shell}}}{c_{DNA} \times \frac{2}{3} \times 3{,}238{,}442{,}024 \times 2.6862\%}} = 13.1708$$

Figure 2: The calculation of the apparent acid dissociation constant of the haploid human genome, and of the interphase intranuclear micro-pH values induced by human genome depending on its intrinsic epigenetic occupation status, (A) the calculation of the apparent (effective) $pK'_{a,HG}$ (25 °C) = 7.1849 of the haploid human genome according to the method of *Katchalsky & Gillis* [25] and *Kuhn & Kuhn* [26] [$pK'_{a,HG}$ = apparent acid dissociation constant (25 °C) of haploid *H. sapiens* genome B-DNA double helix; $pK_{a,R-OH}$ = 1.29 = theoretical pK_a (25 °C) [24] of one isolated internucleotide phosphodiester (R–OH) proton; s = 1 = number of statistical subunits on thread molecule [26]; j = 6 = number of spacing atoms (at least distance) in one dsDNA repeating unit [26]; b = 0.334 × 10^{-7} cm (0.334 ± 0.01 nm [27]) = length rise in cm of one B-DNA repeating unit (helix rise/bp) in solution; h_v = end–to–end distance of dsDNA at half-neutralization; h_0 = end–to–end distance of dsDNA], (B) the theoretical micro-pH [77] values surrounding *H. sapiens* haploid (and diploid) interphase euchromatin were calculated as the intranuclear micro-pH induced by human haploid (and diploid) genome treated as a weak acid, from pH_{DNA}, $pH_{spermine}$, and pH_{shell}, by applying the formula for

Preprints (www.preprints.org) | NOT PEER-REVIEWED | Posted: 4 December 2017 doi:10.20944/preprints201701.0086.v3

pH induced by weak acids: $pH = -\log_{10}(K_s \times c_s)$, or the formula for pH induced by weak bases: $pH = -\log_{10}[(K_w \times K_s) \times (c_s)^{-1}]$ (K_s, acid dissociation constant; $K_w = 10^{-14}$). The intranuclear micro-pH was calculated by the law for the calculation of the solution pH induced by salts of weak acids with weak bases: $pH_{salt} = 0.5 \times (pH_{acid} + pH_{base})$.

Preprints (www.preprints.org) | NOT PEER-REVIEWED | Posted: 4 December 2017 doi:10.20944/preprints201701.0086.v3

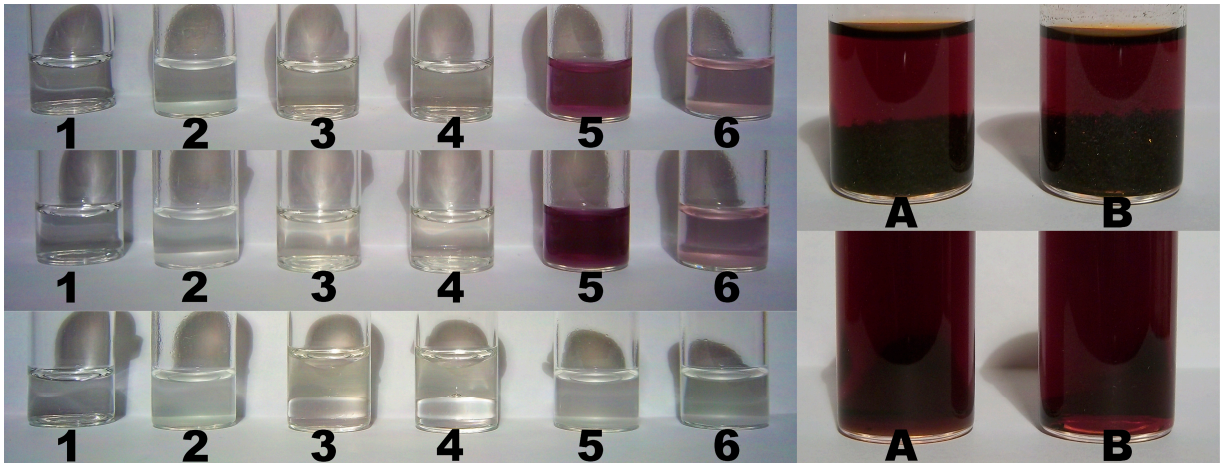

Figure 3: Color assays for cyclo-O_8-Na^+ contained in **RC**, for the destruction of cyclo-O_8-Na^+ by the glyphosate metabolite (aminomethyl)phosphonic acid (AMPA) (left, **1**–**6**), and for the potential reduction of elemental iodine by AMPA (right, **A** and **B**). Solutions (left, **1**–**6**) were: KI (**1**), KI + starch (**2**), **RC** + KI (**3**), **RC** + KI + AMPA (**4**), **RC** + KI + starch (**5**), and **RC** + KI + starch + AMPA (**6**). The concentrations in solution were: **RC**, 16.95 mM (with cyclo-O_8-Na^+, 67.79 mM); KI, 156.63 mM; AMPA, 99.06 mM. The solutions were incubated at two room temperatures for prolonged time. Afterwards (left, bottom row), both **RC** + KI (**3**) and **RC** + KI + AMPA (**4**) were extracted with deuterated chloroform (bottom phase), and (left, bottom row) both **RC** + KI + starch (**5**) and **RC** + KI + starch + AMPA (**6**) were treated with L-ascorbic acid. Legend: left, top row (**1**–**6**) = first photograph series; left, middle row (**1**–**6**) = second photograph series; left, bottom row (**1**–**6**) = third photograph series; right, top row (first photograph series): (**A**) AMPA (76.55 mM) + iodine (as I_2, 78.80 mM), (**B**) iodine (as I_2, 78.80 mM); right, bottom row (second photograph series): (**A**) AMPA (51.03 mM) + iodine (as I_2, 52.53 mM), (**B**) iodine (as I_2, 52.53 mM).

Preprints (www.preprints.org) | NOT PEER-REVIEWED | Posted: 4 December 2017 doi:10.20944/preprints201701.0086.v3

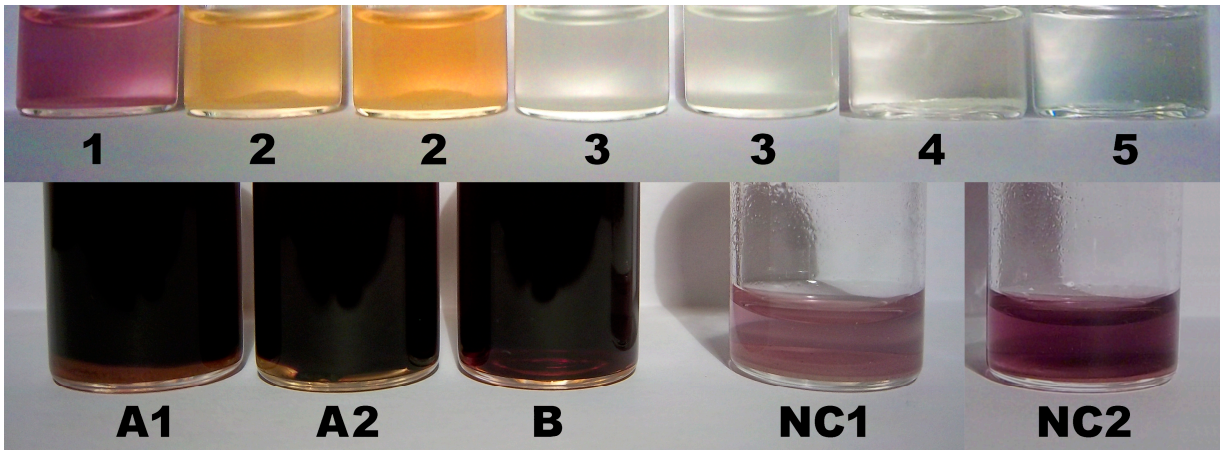

Figure 4: Color assays for the destruction of cyclo-O_8-Na^+ contained in **RC** by glyphosate and ROUNDUP® GRAN (top, **1**–**5**), for the potential reduction of elemental iodine by glyphosate and ROUNDUP® GRAN (bottom, **A1**, **A2**, and **B**), and for cyclo-O_8-Na^+ contained in **NC** (bottom, **NC1** and **NC2**). Solutions (top, **1**–**5**) were: **RC** + KI + starch (**1**), **RC** + KI + starch + glyphosate (free acid) (**2**), **RC** + KI + starch + ROUNDUP® GRAN (**3**), **RC** + KI + glyphosate (free acid) (**4**), and **RC** + KI + ROUNDUP® GRAN (**5**). The concentrations in solution were: **RC**, 16.95 mM (with cyclo-O_8-Na^+, 67.79 mM); KI, 171.69 mM; glyphosate, 100.55 mM; glyphosate-Na, 108.15 mM. The solutions were incubated at two room temperatures for prolonged time. Legend (bottom): (**A1**) glyphosate (free acid, 102.52 mM) + iodine (as I_2, 98.50 mM), (**A2**) ROUNDUP® GRAN (glyphosate-Na, 102.77 mM) + iodine (as I_2, 98.50 mM), (**B**) iodine (as I_2, 98.50 mM), (**NC1**, **NC2**) **NC** (18.25 mM, with cyclo-O_8-Na^+, 18.25 mM) + KI (259.04 mM) after 10 h (**NC1**) and 50 h (**NC2**) incubation.

Preprints (www.preprints.org) | NOT PEER-REVIEWED | Posted: 4 December 2017 doi:10.20944/preprints201701.0086.v3

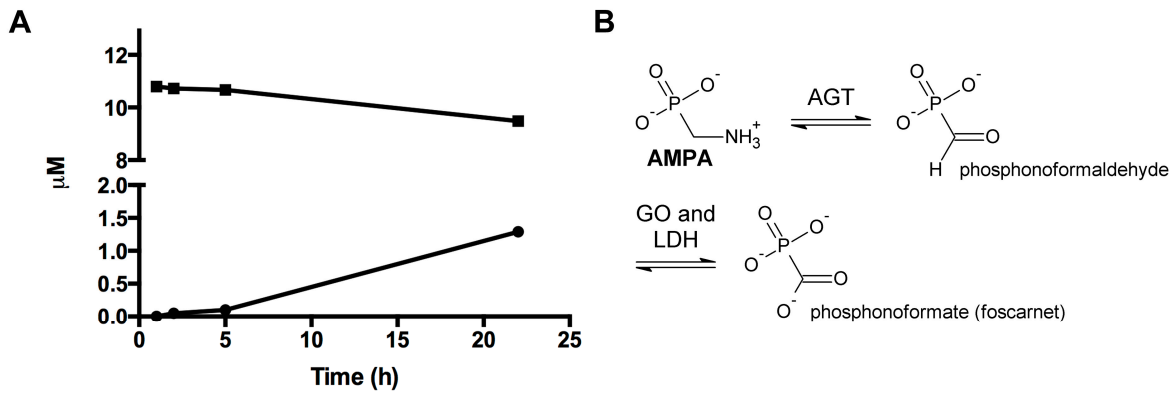

Figure 5: The catabolism of AMPA by human peroxisomal alanine:glyoxylate aminotransferase (AGT), (A) time course of the AMPA half-transamination reaction of human AGT. The enzyme at a concentration of 5 µM was incubated at 25 °C in 100 mM potassium phosphate buffer (pH 7.4). At the indicated times, aliquots were withdrawn and denatured. After removal of the precipitated protein by centrifugation, the supernatants were subjected to HPLC analysis (squares, PLP; circles, PMP), (B) the generation of phosphonoformate (foscarnet) from AMPA over the intermediate phosphonoformaldehyde by the rate-limiting transamination of the major environmental glyphosate metabolite AMPA. Phosphonoformaldehyde, seen as an glyoxylate analogue, could be oxidized by glycolate oxidase (GO) and lactate dehydrogenase (LDH) [90]. Foscarnet is a potent inhibitor of eukaryotic DNA polymerase α [91,92], an enzyme crucially involved in maintaining chromosomal integrity and telomere length [93].

Preprints (www.preprints.org) | NOT PEER-REVIEWED | Posted: 4 December 2017 doi:10.20944/preprints201701.0086.v3

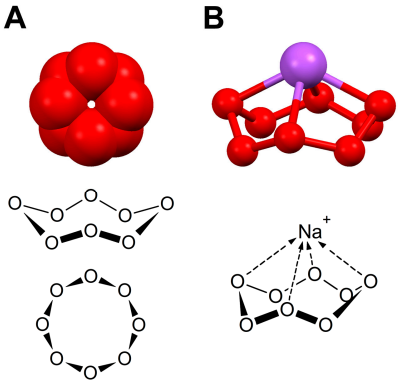

Figure 6: Molecular modeling of cyclooctaoxygen (cyclo-O_8) and its Na^+ complex [5], performed with ACD/Chem Sketch version 12.01 with integrated ACD/3D Viewer (Advanced Chemistry Development, Inc., Toronto, Ontario, Canada) and processed with Mercury 3.1 version 3.1.1 [The Cambridge Crystallographic Data Centre (CCDC), Cambridge, United Kingdom], (A) the cyclo-O_8 octagon (top, space-fill model; middle, crown conformation in D_{4d} symmetry; bottom, octagon), (B) molecular modeling of the square pyramidal (*SPY*-4)-cyclo-O_8-Na^+ crown complex.

Preprints (www.preprints.org) | NOT PEER-REVIEWED | Posted: 4 December 2017 doi:10.20944/preprints201701.0086.v3

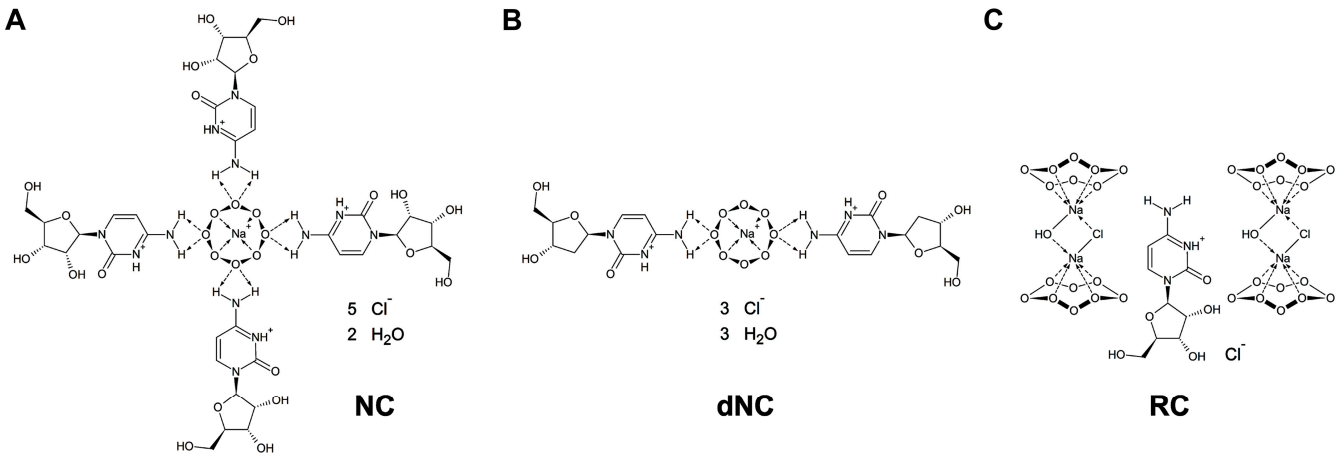

Figure 7: The chemical structures of cyclo-O_8-Na^+-containing complexes [5], (A) the cyclo-O_8-Na^+-containing complex **NC** synthesized by refluxing cytidine × HCl with ninhydrin under influence of atmospheric O_2, (B) the cyclo-O_8-Na^+-containing complex **dNC** synthesized by refluxing 2'-deoxycytidine × HCl with ninhydrin under influence of atmospheric O_2, (C) the cyclo-O_8-Na^+-containing complex **RC** synthesized by biomimetic reaction with buffered 3% H_2O_2 as catalysed (catalase effect) by *Candida utilis* low-molecular weight RNA and $NaHCO_3$ at ambient temperature and physiological pH.

Preprints (www.preprints.org) | NOT PEER-REVIEWED | Posted: 4 December 2017 doi:10.20944/preprints201701.0086.v3

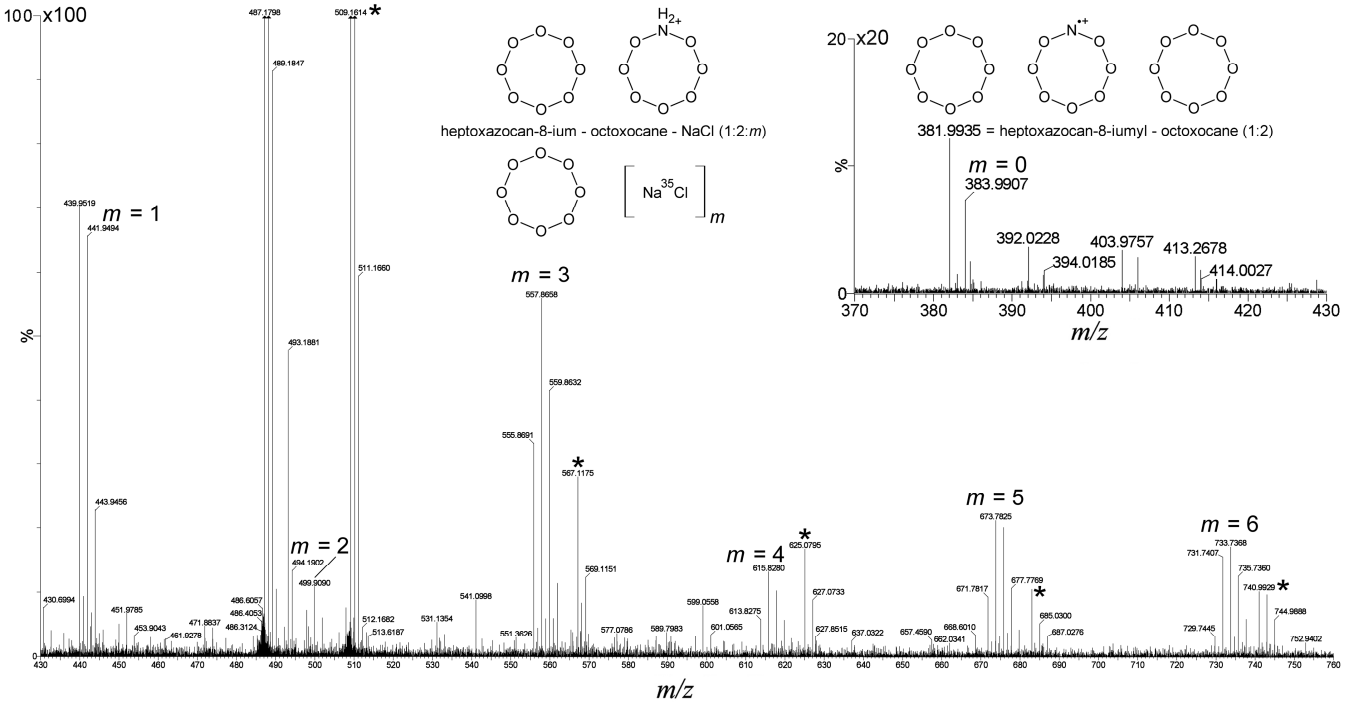

1332 **Figure 8:** Electrospray ionization mass spectrometry of **RC** [5]. Magnified (100 ×)
1333 section of the ESI–MS spectrum of **RC** dissolved in H_2O/methanol from *m*/*z* 430 to *m*/*z*
1334 760. Inset, magnified (20 ×) segment of the ESI–MS spectrum of **RC** from *m*/*z* 370 to
1335 *m*/*z* 430. The cluster cations of heptoxazocan-8-ium – octoxocane – $Na^{35}Cl$ (1:2:*m*) are
1336 marked (*m* = 0–6). Not marked are the +2 isotope peaks resulting from ^{37}Cl instead of
1337 one ^{35}Cl (*m* = 1–6). The origin of the heptoxazocan-8-iumyl – octoxocane (1:2) cluster
1338 radical cations (–2 peaks) is indicated in the inset. The cluster cations of $[(cytidine)_2$ +
1339 Na + $(NaCl)_n]^+$ (*n* = 0–5) are marked with stars.

Preprints (www.preprints.org) | NOT PEER-REVIEWED | Posted: 4 December 2017 doi:10.20944/preprints201701.0086.v3

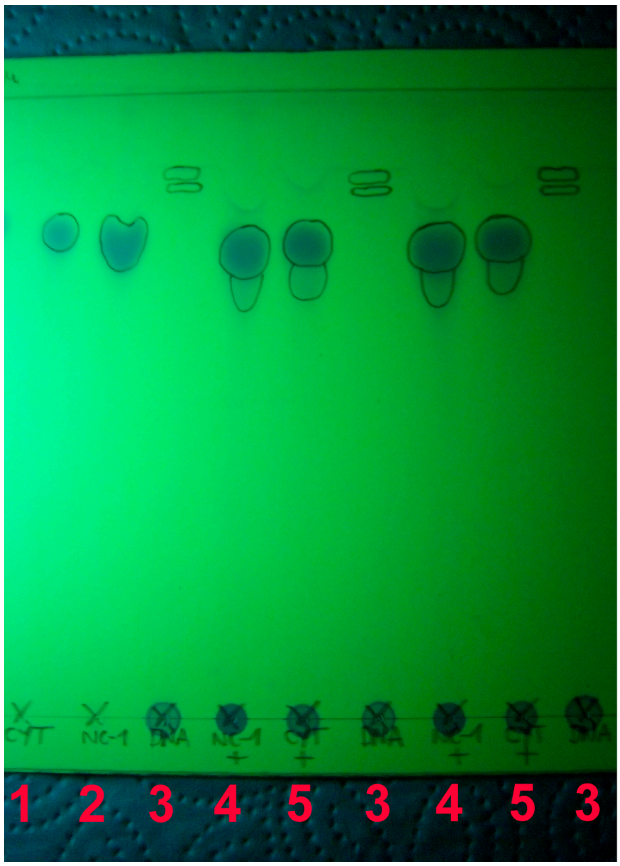

← Eluent front

← 587 nt
← 831 nt
} ← Salmon testes ssDNA fragments (created by sonication) (3), and salmon testes ssDNA complexation bulges (4, 5)

} ← Cytidine × HCl (1), NC (2), cytidine × HCl complexed with salmon testes ssDNA (5), cytidine × HCl complexed with salmon testes ssDNA which itself is complexed with cyclooctaoxygen–Na^+ [(octoxocane-κ^4O^1,O^3,O^5,O^7)sodium(1+)] (4)

← Re-annealed salmon testes double-stranded DNA (dsDNA) (3, 4, 5)

Figure 9: Thin-layer chromatographic mobility shift assay of the binding of **NC** to salmon testes ssDNA fragments (sonicated salmon testes genomic DNA) [5], (1) cytidine × HCl, incubation at RT for 1 h 15 min, 40 µl solution on spot, (2) **NC**, incubation at RT for 1 h 15 min, 40 µl solution on spot, (3) salmon testes ssDNA, 100 µl salmon testes ssDNA colloidal stock solution diluted with 300 µl H_2O, incubation at RT for 55 min, 80 µl colloidal solution on spot, (4) salmon testes ssDNA + **NC**, 700 µl salmon testes ssDNA colloidal stock solution added to 500 µl of **NC** stock solution, incubation at RT for 1 h, 80 µl colloidal solution on spot, (5) salmon testes ssDNA + cytidine × HCl, 200 µl salmon testes ssDNA colloidal stock solution added to 500 µl of cytidine × HCl stock solution, incubation at RT for 1 h, 80 µl colloidal solution on spot.

Preprints (www.preprints.org) | NOT PEER-REVIEWED | Posted: 4 December 2017 doi:10.20944/preprints201701.0086.v3

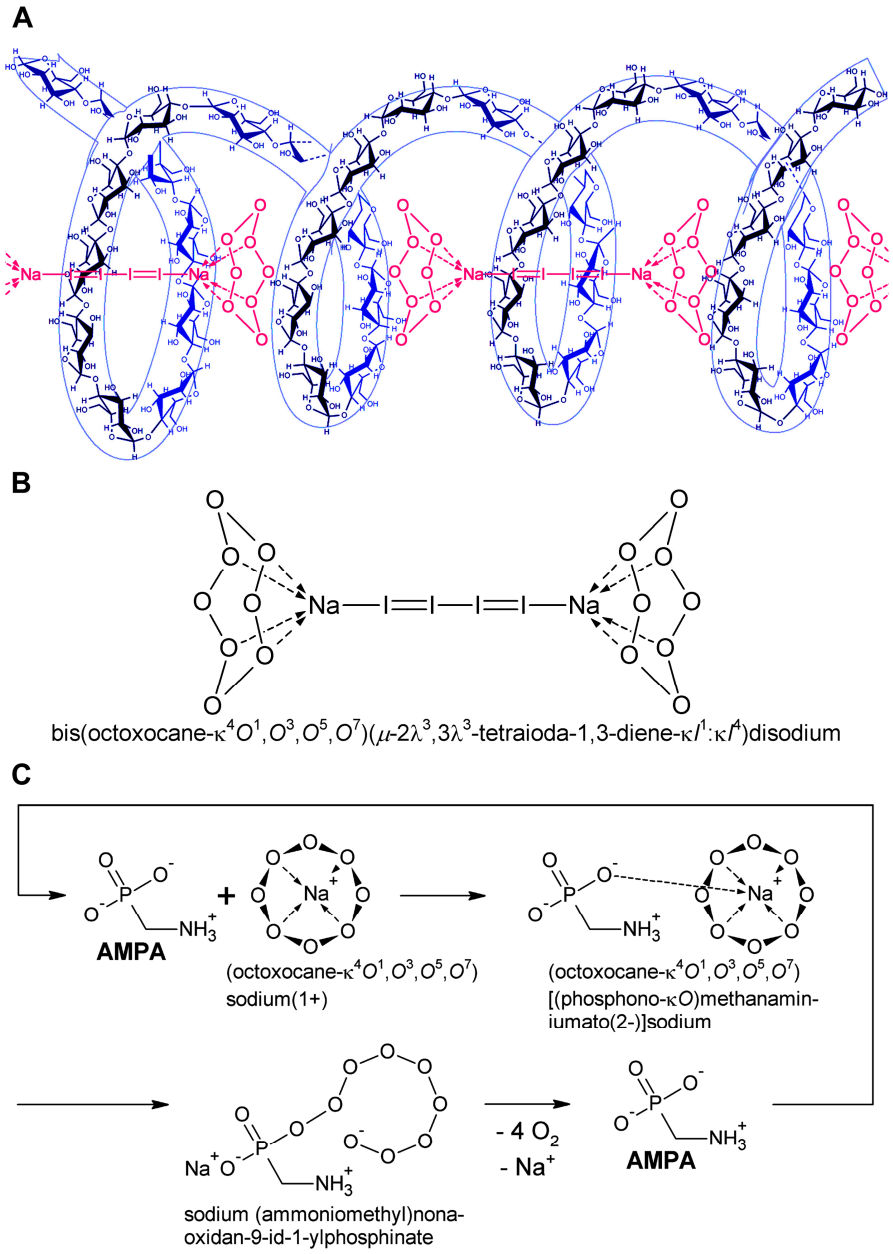

Figure 10: Explanation of the color reaction for cyclo-O_8-Na^+ contained in **RC**, and the destruction of cyclo-O_8-Na^+ by the glyphosate metabolite (aminomethyl)phosphonic acid (AMPA), (A) the cyclo-O_8-Na^+ complex contained in **RC** reacted with potassium iodide under catalysis by potato starch to an intensely colored (reddish violet) [(cyclo-O_8-Na^+)$_2$(I_4^{2-})] complex stabilized within the starch-contained amylose helix, (B) the

Preprints (www.preprints.org) | NOT PEER-REVIEWED | Posted: 4 December 2017 doi:10.20944/preprints201701.0086.v3

proposed chemical formula for the amylose-complexed [(cyclo-O_8-Na^+)$_2$(I_4^{2-})]: bis(octoxocane-κ^4O^1,O^3,O^5,O^7)(μ-2λ^3,3λ^3-tetraioda-1,3-diene-κI^1:κI^4)disodium, (C) a logically deduced catalytic 'rolling-circle' mechanism for the AMPA-catalysed degradation of cyclo-O_8-Na^+. The cycloocytooxygen ring is split to a phosphonate-esterified nonaoxidanide which is stabilized by ionic binding to the primary ammonium cation of AMPA. The phosphonate-esterified nonaoxidanide eliminates four oxygen O_2 molecules by a 'rolling-circle' cascade, regenerating AMPA.

Preprints (www.preprints.org) | NOT PEER-REVIEWED | Posted: 4 December 2017 doi:10.20944/preprints201701.0086.v3

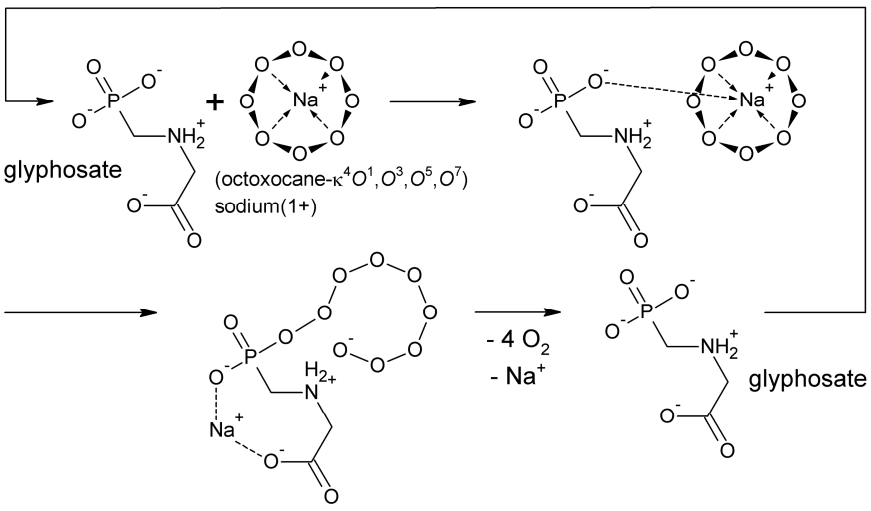

Figure 11: A logically deduced catalytic 'rolling-circle' mechanism for the (fully ionized) glyphosate-catalysed degradation of cyclo-O_8-Na^+. The cycloocytooxygen ring is split to a phosphonate-esterified nonaoxidanide which is stabilized by ionic binding to the secondary ammonium cation of glyphosate (and complexation of the sodium cation). The phosphonate-esterified nonaoxidanide eliminates four oxygen O_2 molecules by a 'rolling-circle' cascade, regenerating glyphosate.

Preprints (www.preprints.org) | NOT PEER-REVIEWED | Posted: 4 December 2017 doi:10.20944/preprints201701.0086.v3

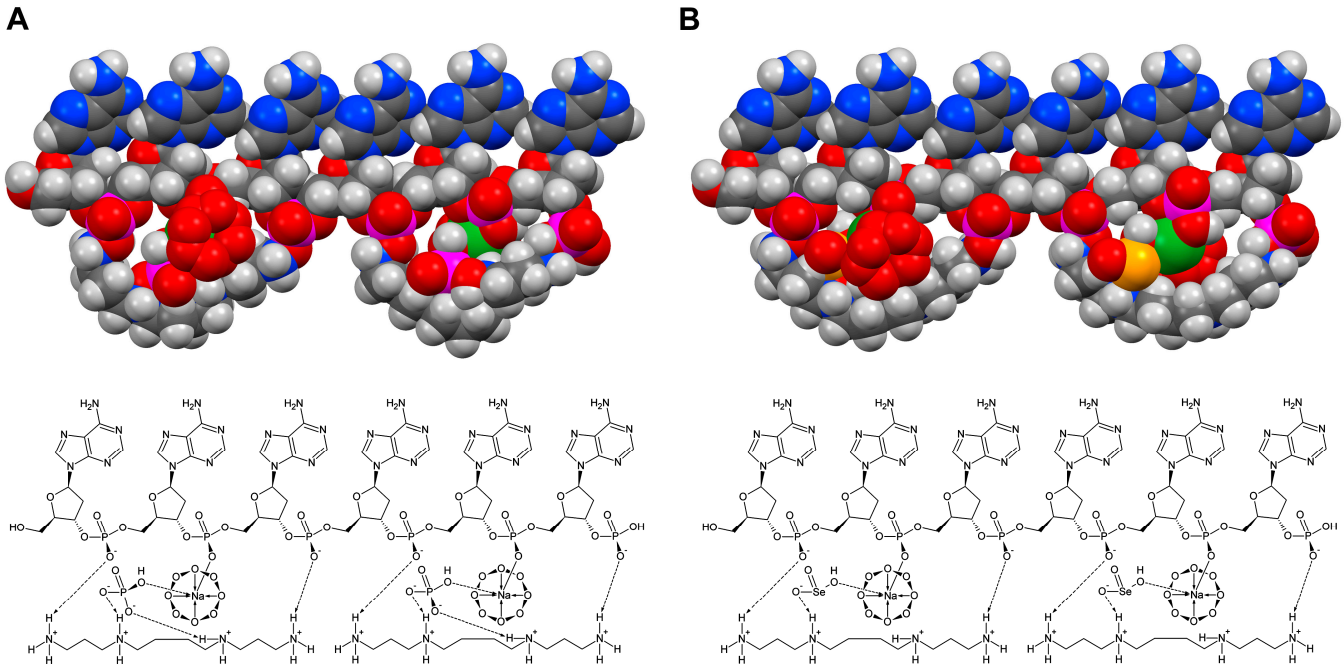

Figure 12: Molecular modeling [ACD/Chem Sketch version 12.01 with integrated ACD/3D Viewer (Advanced Chemistry Development, Inc., Toronto, Ontario, Canada), Mercury 3.1 version 3.1.1 (The Cambridge Crystallographic Data Centre, Cambridge, United Kingdom)] of the postulated [5] first epigenetic shell of euchromatic *in vivo* DNA, as exemplified for a single-stranded hexanucleotide, introducing a molecular biological model for sperminium phosphate/cyclo-O_8-Na^+/ssDNA and sperminium selenite/cyclo-O_8-Na^+/ssDNA interactions, (A) the molecular model of the single-stranded hexanucleotide d(ApApApApApAp) liganded with cyclo-O_8-Na^+ and sperminium phosphate, (B) the molecular model of d(ApApApApApAp) liganded with cyclo-O_8-Na^+ and sperminium selenite. Element color codings for (A) and (B): gray, carbon; white, hydrogen; blue, nitrogen; red, oxygen; purple, phosphorus; green, sodium; yellow, selenium.

Preprints (www.preprints.org) | NOT PEER-REVIEWED | Posted: 4 December 2017 doi:10.20944/preprints201701.0086.v3

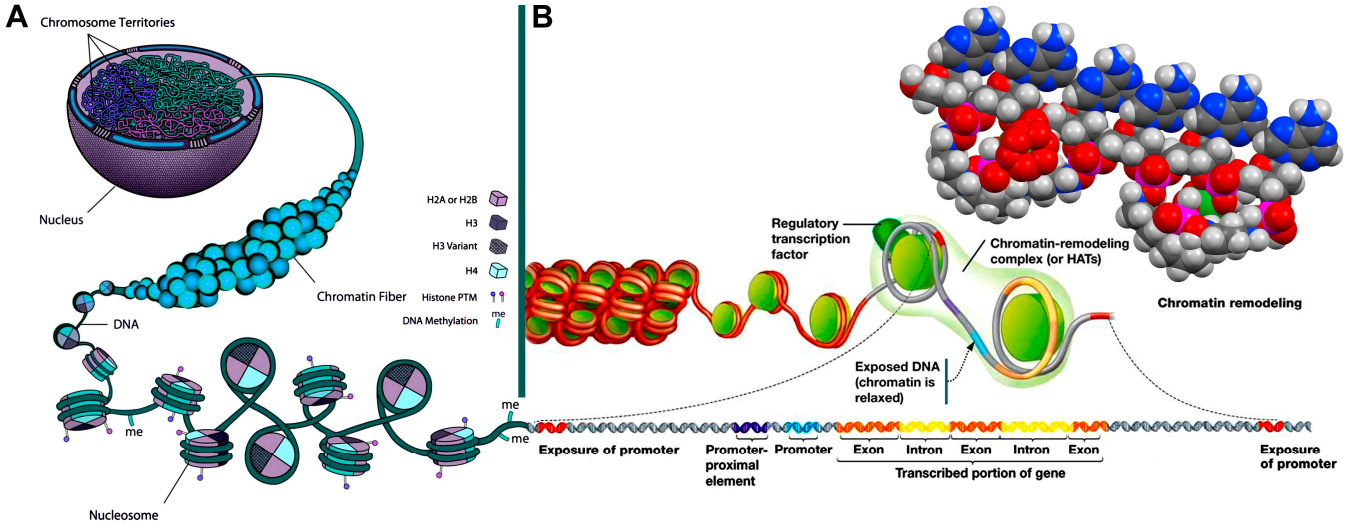

1380 **Figure 13:** An improved and corrected model for the cyclooctaoxygen sodium-bridged
1381 spermine phosphate (and selenite) epigenetic shell [5] of actively transcribed gene
1382 regions in eukaryotic interphase 'open' chromatin DNA, (A) the nucleus of an eukaryotic
1383 cell with chromosome territories, chromatin fiber (10 nm 'beads–on–a–string' fiber),
1384 nucleosome structure, nucleosome octamer core histone proteins [H2A/H2B, H3/H3
1385 variant, H4] with posttranslational histone protein modifications (histone PTM), and
1386 decondensing DNA with regulative cytosine nucleobase 5-methylation sites (me).
1387 Adapted and modified in part from [96], (B) the decondensation of chromatin enabling
1388 gene transcription in eukaryotic interphase 'open' chromatin DNA. The relaxed
1389 chromatin, regulatory transcription factor, chromatin-remodeling complex/histone acetyl
1390 transferases (HATs), and chromatin remodeling are indicated. The 'open' DNA with the
1391 transcription-prone gene is generally structured in promoter, promoter-proximal genetic
1392 elements, transcribed/expressed gene exons and non-expressed gene introns. The
1393 cyclooctaoxygen sodium-bridged spermine phosphate (and selenite) epigenetic
1394 coverage of this actively transcribed gene region is symbolized.

Preprints (www.preprints.org) | NOT PEER-REVIEWED | Posted: 4 December 2017 doi:10.20944/preprints201701.0086.v3

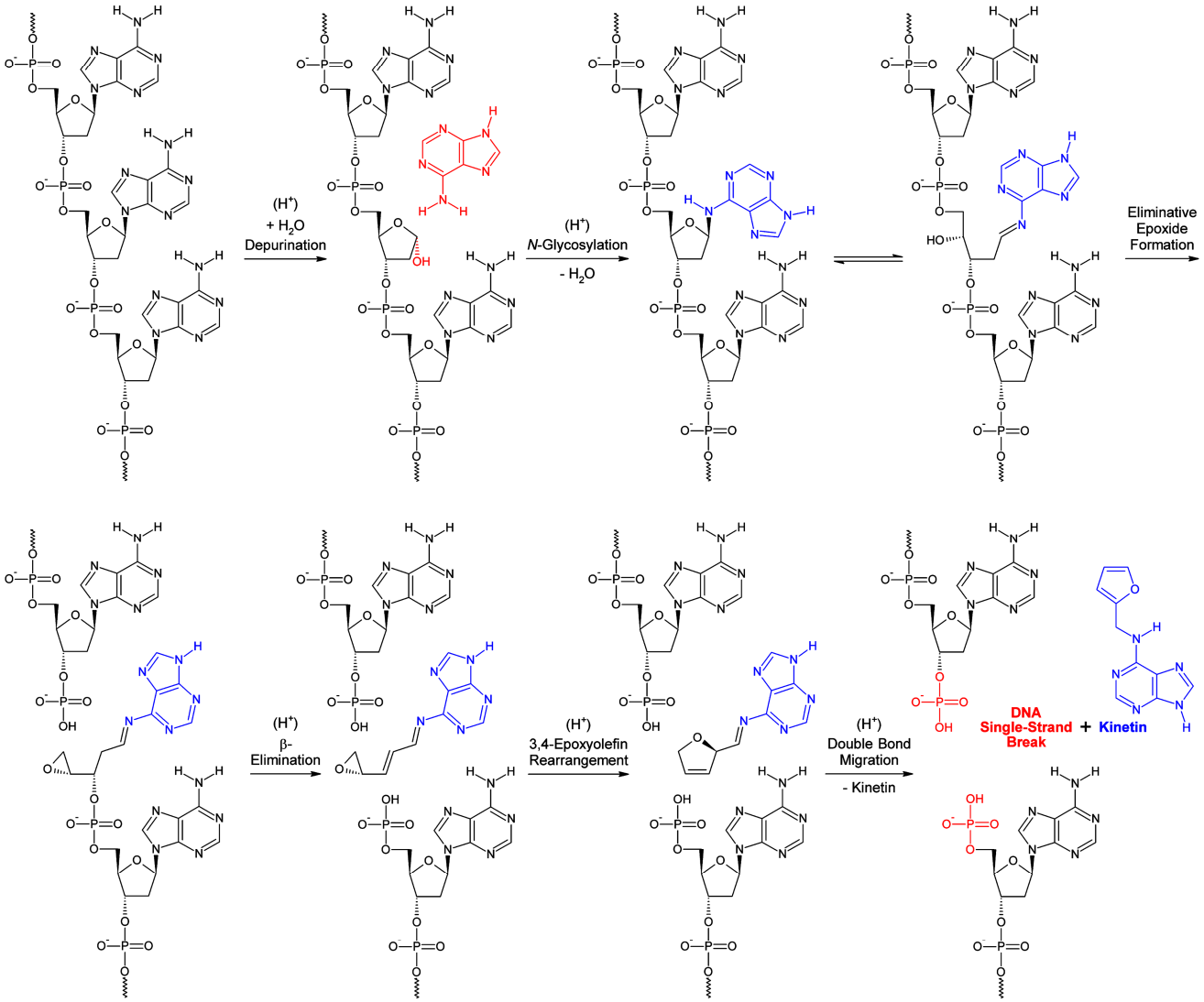

Figure 14: A chemical mechanistic deduced logical scheme for the generation of kinetin (N^6-furfuryl-9*H*-adenine) [107] from DNA by proton catalysis (kinetin-generating "base flip", KGBF). Protonation of the adenine nucleobase of the shown d(pAp**A**pAp) sequence at purine N-7 induces depurination [104,105], creating an apurinic site [104–106]. Proton-catalysed *N*-glycosylation [110,111] at the 6-NH_2 of adenine regenerates a nucleobase-inverted 2'-deoxynucleotide which is in furanose ring-opening equilibrium with its ald(os)imine form. Two eliminations simultaneously follow, the first (auto-catalysed by 3'-*O*-phosphate conjugate base proton reception) by S_N2-nucleophilic

Preprints (www.preprints.org) | NOT PEER-REVIEWED | Posted: 4 December 2017 doi:10.20944/preprints201701.0086.v3

eliminative epoxide formation, the second by proton-catalysed (auto-catalysed by the previously liberated 3'-*O*-monohydrogen phosphate conjugate acid) β-elimination (E1 unimolecular elimination), which leads to an 3,4-epoxyolefin: *N*-{(1*E*,2*E*)-3-[(2*S*)-oxiran-2-yl]prop-2-en-1-ylidene}-9*H*-purin-6-amine. The chiral (*S*)-2-vinyloxirane structure rearranges to a chiral (*R*)-2-alkyl-2,5-dihydrofuran due to 3,4-epoxyolefin rearrangement [112,113]: *N*-[(2*R*)-2,5-dihydrofuran-2-ylmethyl]-9*H*-purin-6-amine. The latter compound rearranges to kinetin through facile double bond migration driven by aromatization to a furan. A DNA single-strand break is left back.